Environmental Modelling & Software 74 (2015) 1–20

Contents lists available at ScienceDirect

Environmental Modelling & Software

journal homepage: www.elsevier.com/locate/envsoft

Simulating the influences of groundwater on regional geomorphology using a distributed, dynamic, landscape evolution modelling platform

Andrew Barkwith [a, *], Martin D. Hurst [a], Christopher R. Jackson [a], Lei Wang [a], Michael A. Ellis [a], Tom J. Coulthard [b]

[a] British Geological Survey, Environmental Science Centre, Keyworth, Nottingham, NG12 5GG, UK
[b] Department of Geography, Environment and Earth Science, University of Hull, Cottingham Road, Hull, HU6 7RX, UK

ARTICLE INFO

Article history:
Received 22 May 2015
Received in revised form
28 August 2015
Accepted 1 September 2015
Available online xxx

Keywords:
Cellular automata
Sediment transport
Groundwater
Landscape evolution
CAESAR-Lisflood
CLiDE

ABSTRACT

A dynamic landscape evolution modelling platform (CLiDE) is presented that allows a variety of Earth system interactions to be explored under differing environmental forcing factors. Representation of distributed surface and subsurface hydrology within CLiDE is suited to simulation at sub-annual to centennial time-scales. In this study the hydrological components of CLiDE are evaluated against analytical solutions and recorded datasets. The impact of differing groundwater regimes on sediment discharge is examined for a simple, idealised catchment, Sediment discharge is found to be a function of the evolving catchment morphology. Application of CLiDE to the upper Eden Valley catchment, UK, suggests the addition of baseflow-return from groundwater into the fluvial system modifies the total catchment sediment discharge and the spatio-temporal distribution of sediment fluxes during storm events. The occurrence of a storm following a period of appreciable antecedent rainfall is found to increase simulated sediment fluxes.

© 2015 Published by Elsevier Ltd.

Software availability

Name of software: CLiDE
Developer: Andrew Barkwith
Contact address: British Geological Survey, Environmental Science Centre, Keyworth, Nottingham, NG12 5GG, UK. E-mail: andr3@bgs.ac.uk
Year first available: 2013
Required software: Windows
Program Language: C#
Availability and cost: GNU licensed freeware

1. Introduction

1.1. Cellular automata

Simulation of distributed dynamic environmental systems is often based on the solution of differential equations that can be difficult to solve without simplification (Toffoli, 1984) or large computational resources. Cellular automata (CA), first developed by von Neumann (1951, 1966) to investigate self replication, provided an alternative to solving the governing equations, allowing a fast, exact numerical simulation of a physical system. Since their inception CA have been applied to a host of physical research areas focussed around fluid dynamics and natural systems (see for example, Margolus et al., 1986; Somers, 1993; Chen and Doolen, 1998; Chopard and Masselot, 1999). CA discretises space into regular two- or three-dimensional cells, each of which contain physical property information for that region of space. Each cell is able to pass and gather information about neighbouring cells and subsequently modify its contents based on a transfer function. Interaction with neighbouring cells for two-dimensional cases usually consists of either a Moore-type method, where all surrounding cells interact with the central node, or a von Neumann (Manhattan) neighbour-type method where interaction is solely with adjacent cells (Fig. 1). Initial cell states are user defined, and with each time step states are simultaneously updated based on the transfer function and states of neighbouring cells.

1.2. Groundwater and geomorphology

The impacts of surface hydrological processes on geomorphology, and thus topography, have been studied using

* Corresponding author.
E-mail address: andr3@bgs.ac.uk (A. Barkwith).

http://dx.doi.org/10.1016/j.envsoft.2015.09.001
1364-8152/© 2015 Published by Elsevier Ltd.

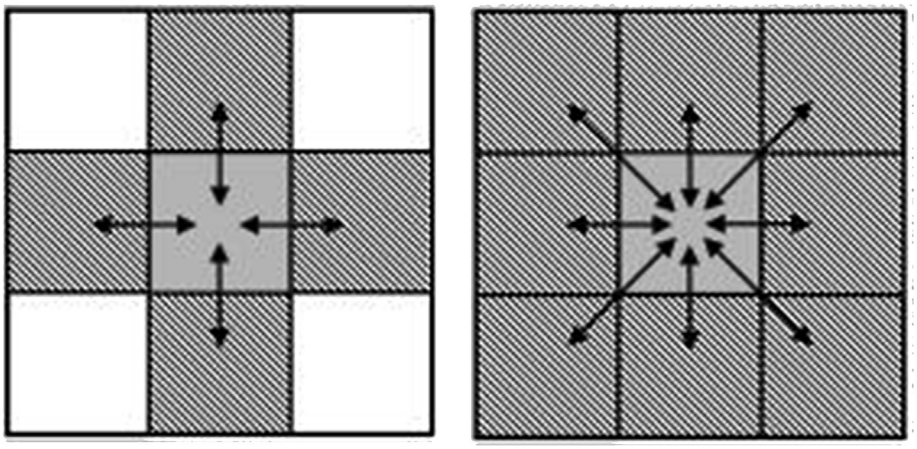

Fig. 1. CA neighbourhoods; the von Neumann neighbourhood (left) considers cells in the cardinal directions and the Moore neighbourhood (right) allows interactions with all immediate cells. Arrows represent cell neighbourhood interaction with a central node.

numerical methods for a number of years. With advances in computer processing power available to researchers, the development of landscape evolution models (LEMs) has progressed from simulating water routing effects on nodal elevation (Ahnert, 1976), to representing detailed fluvial and hillslope processes (for a full review see Tucker and Hancock, 2010). Recent advances in this field have seen increases in domain sizes and resolution, irregular gridding techniques, and the move from hypothetical to real catchments becoming common place (e.g., Pazzaglia, 2003; Coulthard et al., 2012). Currently, LEMs based on regular, square, gridded digital elevation models (DEM) are popular as slope attribution does not need to be determined manually. These DEM-based models also have the advantage of allowing run-time landscape adjustment in response to runoff, erosion and deposition (Hancock et al., 2011). Current models contain representations of surface hydrology but they all either use highly simplified representations of groundwater influx to rivers (as a constant baseflow) or ignore groundwater processes entirely (Huang and Niemann, 2006). An exception to this is Keesstra et al. (2014), who capture the transient nature of baseflow in an LEM environment suitable for simulating relatively small catchments.

There are a number of mechanisms by which groundwater can have an impact on erosional processes. Within cohesive soils or sediments, in a process similar to overland flow, the formation of subsurface channels from groundwater scour can cause near-surface fractures or cracks in the overlying surface (Dunne, 1988). These pipes can collapse, leading to the formation of extensive gully networks. This process tends to occur in shale-dominated, arid or semi-arid regions (Howard and McLane, 1988). The seepage of groundwater to the surface can locally enhance the erodibility of cohesive soils or sediments by increasing their susceptibility to a range of physical and chemical weathering processes (Laity and Malin, 1985). Chemical weathering at depth, which subsequently leads to enhanced erosion when a unit is exposed, can also be attributed to groundwater processes (Kelly, 2012). In less cohesive sediments the seepage of groundwater to the surface can provide buoyancy to particles, reducing the flow velocities required to entrain them and increasing the development of channel features (Fox et al., 2007). Groundwater flow operates on longer temporal scales than direct surface runoff and, in its simplest form, introduces a mechanism to lag surface water flow and impart a smoothing effect on surface fluvial systems (Changnon et al., 1988). Through this process, the fluvial flow velocities that drive sediment flux can be modified at multiple spatio-temporal scales.

Due to the limited extent of tunnel-scour erosion and long timescales associated with physical and chemical weathering, these processes are not considered in this study, which focusses on sub-annual to centennial geomorphological evolution. Although the groundwater seepage buoyancy process is known to be important locally, the impact on differing sediment classes and under differing groundwater regimes is not well constrained. Due to its conceptual simplicity and potential applications, it is the representation of baseflow-return to the fluvial system and the impacts that this can have on catchment morphology and sediment transport that forms the basis of this study.

1.3. Baseflow

The time taken for water to enter the groundwater system through recharge, until its contribution to a surface water body as baseflow, is influenced significantly by topography, geology, vegetation, land use and climate factors. Aquifer recharge through channel infiltration during storm events can be large enough to modify the commonly observed power law relationship between discharge and basin area (Goodrich et al., 1997), although many LEMs assume this relationship to be linear. If the return of this water to the surface as baseflow coincides with future rainfall events, the increase in storm flow can be significant (Sklash and Farvolden, 1979; Buttle, 1994; Kirchner et al., 2000). Spatial variability of baseflow is generally highly heterogeneous across a catchment, often increasing surface river flows in the lower reaches. The combination of these spatial and temporal groundwater influences on surface water dynamics can create a highly complex system. Modelling surface water flow dynamics accurately under these complex hydrological conditions without a groundwater component is often not possible. The characteristics of catchments with greatest susceptibility to complex hydrological interactions are: those with large ranges between topographic highs and lows, creating a strong subsurface hydraulic flow gradient; those with highly heterogeneous hydraulic conductivity and specific yield, formed for example by changes in geology; those where groundwater exhibits a strong seasonal signal and hence a variable baseflow-return to rivers, for example sandstone aquifers; and those that are unconfined, allowing the return of water to the surface.

1.4. Application

Depending on the baseflow contribution to surface flow components, groundwater process could have major impacts on the

development of terrestrial landscapes at a range of scales. If the focus of a particular study is on representing catchment discharges at time-scales beyond millennia, average values could justifiably be used within LEMs to represent the baseflow components in river flow for a simple groundwater dominated catchment. However, there are situations where the spatial and temporal addition of baseflow-return could be too complex to represent using catchment wide, temporal averages, as they are likely to be highly variable at the sub-annual scale and potentially nonlinear in nature. These occur: at shorter time-scales (centennial and below), where variability of storm events becomes important; in complex groundwater situations; or where the spatial distribution of morphological change is of critical importance to a study.

In this study we describe the development of distributed surface and subsurface hydrological components for a LEM designed to operate at sub-annual to the centennial time-scales. The hydrological components of the resultant modelling platform are verified against analytical solutions. A sensitivity analysis of morphological change under differing groundwater regimes in a small, uniform idealised catchment is subsequently undertaken using the platform to assess the groundwater impacts on fluvial and sediment discharge. Finally the platform is applied to a heterogeneous catchment in north-west England where we examine the role that baseflow plays in controlling sub-annual to decadal scale fluvial and sediment transport properties that can shape catchment scale geomorphology.

2. CLiDE modelling platform

The Dynamic Environmental Sensitivity to Change (DESC) project at the British Geological Survey, on which this paper is based, couples CA modelling from various backgrounds and has produced the CAESAR-Lisflood-DESC (CLiDE) platform; a geomorphological simulator that allows a variety of Earth system interactions to be explored. This platform is based upon the extension of the well established Cellular Automaton Evolutionary Slope and River (CAESAR) model (Coulthard and Van De Wiel, 2006), CAESAR-Lisflood (Coulthard et al., 2013), which incorporates the Lisflood-FP hydrodynamic model (Bates et al., 2010) to simulate channel and overbank flow. The two-dimensional modular design allows great versatility in the range of simulated spatio-temporal scales to which it can be applied. CAESAR has been used to investigate a variety of sediment transport, erosional and depositional processes under differing climatic and land use pressures in river reaches and catchments (e.g., Hancock et al., 2011). The addition of Lisflood-FP to the code (see Coulthard et al., 2013) improves the representation of surface water flow within the model by incorporating momentum. This allows a non-steady flow solution compared to the steady-state flow models of nearly all other LEMs. As with other LEMs, CAESAR-Lisflood simplifies the representation of some of the hydrological processes and their interactions. Specifically, it does not simulate groundwater flow and groundwater discharge to rivers. To address these limitations, the non-Lisflood-FP controlled surface hydrological processes within the CLiDE platform are replaced with a distributed hydrological model that includes a groundwater model. This groundwater model is coupled to the surface model through the exchange of water as groundwater recharge and baseflow-return to rivers.

The coupling of modules in the CLiDE platform, and their distributed nature, allow inter-disciplinary environmental system feedbacks to be explored at a range of scales. A flow chart outlining platform processes and their interactions is shown in Fig. 2. Initialisation of the CLiDE platform requires a number of input items in the form of either gridded or list based ascii files. Spatially discretised initial model inputs are entered as Cartesian grids, with

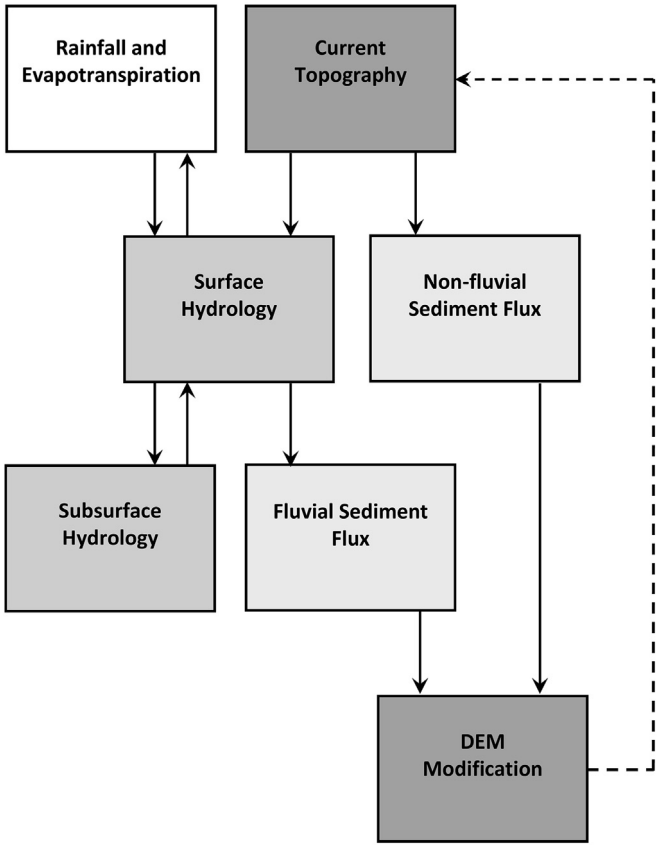

Fig. 2. An overview of the coupled processes in the CLiDE platform. The dashed arrow represents the creation of a new topography at the following time step, when the process is repeated.

header information containing cell size, domain dimensions and geo-referencing details. Distributed DEM, land use, soil hydrological characteristics, daily rainfall and evapotranspiration datasets are used to initialise and force the surface hydrology model. The sediment transport components of the platform use the same DEM as the hydrological components but also require bedrock elevation referenced to the same datum to determine the thickness of the sediment store layer. Grain size distributions, as determined by field measurement or through a calibration process, are required by CLiDE. A detailed characterisation of the sediment transport, vegetation and slope process components used by the CAESAR algorithms in the CLiDE platform is provided by Van De Wiel et al. (2007).

2.1. Hydrological component

Surface and subsurface hydrological processes that ultimately control sediment transport in CLiDE are represented by a distributed coupled CA model. A flow chart of the coupled hydrological components within the platform is presented in Fig. 3. To partition rainfall between evaporatranspiration, surface water runoff and groundwater recharge we implement a soil water balance model (SLiM) based on the conceptualisation of the soil as a single store. Spatially distributed soil types, vegetation types, near surface soil moisture, evapotranspiration and distributed rainfall are considered in calculating the soil water balance and in determining surface water depths and groundwater recharge. Surface water is routed using the Lisflood-FP model (Bates et al., 2010), which takes topographical gradient and terrain frictional proprieties into

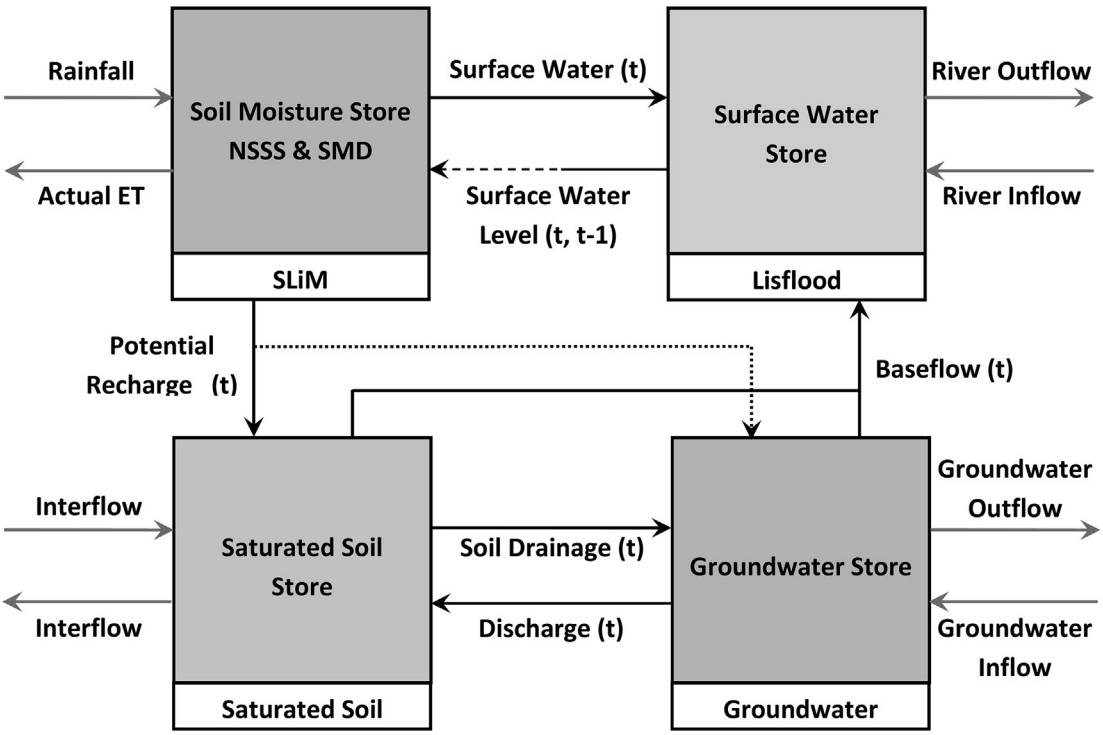

Fig. 3. Diagram representing the coupled surface-subsurface CLiDE hydrological processes. With the exception of rainfall and actual evapotranspiration (ET), arrows not linking processes represent flow between nodes (for example, flow between groundwater nodes). Rainfall inputs into SLiM are defined at model initialisation and actual ET is lost to the atmosphere. The dashed surface water line represents an input from the previous time step and the dotted potential recharge line is shown to avoid confusion with the intersecting baseflow-return line.

account. Subsurface flow is modelled using a two-layer, forward-difference or explicit (Wang and Anderson, 1982), finite difference model, which can be considered as a CA approach (Ravazzani et al., 2011). The upper subsurface layer represents water flow along the bedrock-soil interface (saturated soil in Fig. 3) and the lower layer water within the bedrock (groundwater in Fig. 3). Laterally heterogeneous hydraulic conductivity and specific yield allow versatility in the range of hydrogeological environments that can be represented. The coupled surface-subsurface hydrological component of CLiDE is driven by climate data and constrained by terrain and subsurface properties.

For each of the platform components, space is discretised into uniform, square cells. The soil water balance and groundwater flow model components employ a daily time step, while surface water routing is implemented on an adaptable sub-daily time step. The spatial resolution of the rainfall and potential evapotranspiration datasets for water partitioning should be at the same or coarser resolution than the model resolution, as the code can factor spatial resolutions (from coarser to finer resolution) automatically. If spatial factoring is required, the finer model cells must be coincident (in terms of alignment and the factor used) with the coarser grid, allowing data to be imprinted directly from the lower to higher resolution grid without interpolation.

2.1.1. Soil water balance

We implemented a technique that represents potential groundwater recharge (soil drainage) and runoff processes based on spatio-temporally distributed soil moisture conditions. Soil moisture is influenced by rainfall, potential evapotranspiration, topography, soil type and vegetation (see Fig. 4). Our approach dynamically captures the impact of these processes on soil water properties by responding to variable soil water storage properties (see Rushton, 2003) and vegetation growth stages (see Allen et al., 1998). Within our scheme, rainfall that does not evaporate or contribute directly to runoff can be either intercepted by plants or reach the ground surface and infiltrate into the soil. The latter has the effect of increasing near-surface soil storage and reducing the soil moisture deficit, *SMD* [L]. Soil water can be extracted by plant roots for transpiration or drawn to the bare soil surface for evaporation. When soil moisture reaches field capacity, and the soil is unable to store additional water, water drains freely in the saturated soil.

Additional water inputs to the soil, when field capacity is exceeded, result in the potential for recharge (soil drainage) and lateral surface runoff (routed by Lisflood-FP) if a gradient exists towards adjacent locations. This water, which is not accounted for in soil storage, evapotranspiration or uptake by vegetation is termed *excess water*, E_w [L^3]. Excess water is divided between runoff and recharge to groundwater based on a baseflow index parameter, *BFI* [-], except when the rainfall intensity is greater than the infiltration capacity of soil, where all precipitation is routed as surface runoff (bypass surface runoff in Fig. 4). Baseflow index is an average surface to subsurface water partitioning ratio reflecting the permeable nature of the catchment in addition to other catchment characteristics. The baseflow index parameter may be derived through a calibration process or more commonly is estimated from data by performing a baseflow separation on a river flow time-series (see Eckhardt, 2008). Surface runoff, R_o [L^3], and recharge to the groundwater model, R_e [L^3], are calculated using Eqs. (1) and (2).

$$R_e = E_w \cdot BFI \tag{1}$$

$$R_o = E_w \cdot (1 - BFI) \tag{2}$$

In general, greater runoff and reduced recharge is observed in areas with steeper slopes (see for example, Lange et al., 2003; Haan

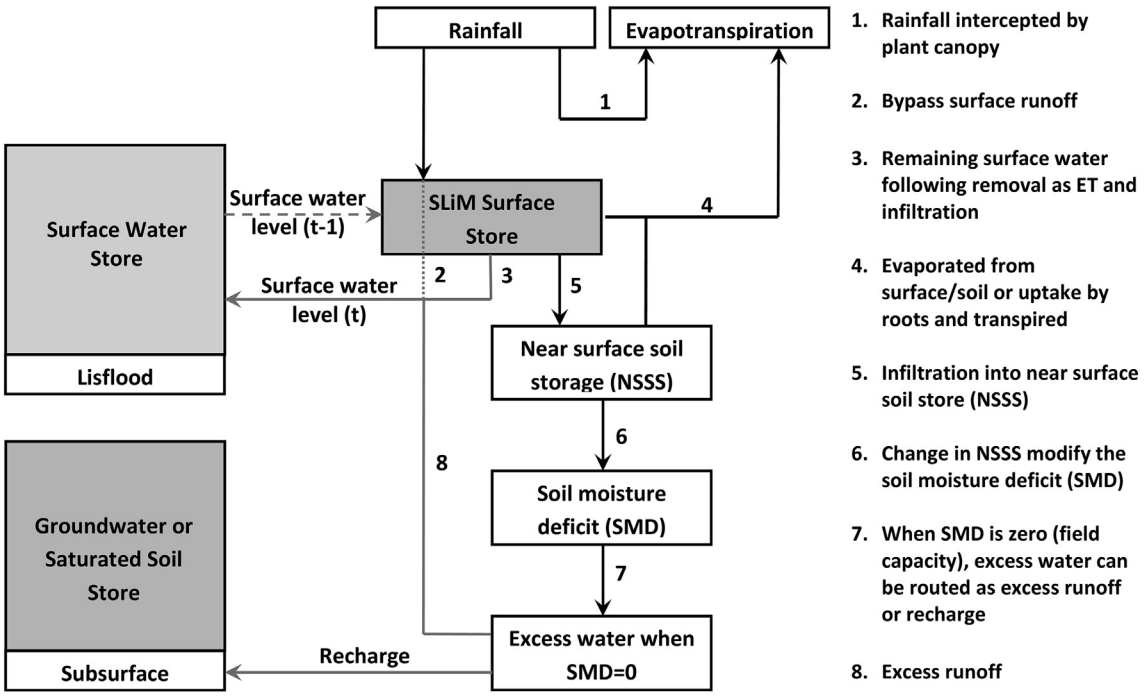

Fig. 4. Flow chart for partitioning of water at the soil surface using the SLiM soil water balance method. Connections with the other water components are included.

et al., 2006). The baseflow index represents a long-term average ratio reflecting, in part, the characteristics of average catchment slope. Runoff and recharge can therefore be understood in terms of how local slope at a particular location compares with a catchment average slope. Consequently Eqs. (1) and (2) can be modified to allow average ($\bar{S}$) and nodal (S) terrain slope [°] to be factored into a calculation of recharge and runoff (Eqs. (3–5)). Using this novel technique, runoff on below average slopes (Eq. (3)) is calculated directly as a function of local to average slope ratio, and runoff on greater than average slopes (Eq. (4)) is a product of catchment runoff for an average slope and that additional amount provided by the local slope angle exceeding this.

$$R_o = \frac{E_w \cdot (1 - BFI) \cdot S}{\bar{S}} \quad \left(\text{if } S \le \bar{S}\right) \tag{3}$$

$$R_o = \frac{\left(S - \bar{S}\right) \cdot E_w \cdot BFI}{\left(90 - \bar{S}\right)} + E_w \cdot (1 - BFI) \quad \left(\text{if } S > \bar{S}\right) \tag{4}$$

$$R_e = E_w - R_o \tag{5}$$

2.1.2. Surface water routing

Routing of surface runoff and channel flow is controlled by a stripped-down version of the Lisflood-FP model (as used by Coulthard et al., 2013). Lisflood-FP is a one-dimensional inertial model that is applied in the x and y directions to simulate flow in two dimensions over a raster grid. To calculate the flow between cells (Q_{sw} [L^3T^{-1}]), Eq. (6) (Bates et al., 2010) is used:

$$Q_{sw} = \frac{q_{sw} - gh_{flow}\Delta t \frac{\Delta(h+z)}{\Delta x}}{\left(1 + gh_{flow}\Delta t n^2 |q_{sw}| \Big/ h_{flow}^{10/3}\right)} \Delta x \tag{6}$$

Here q_{sw} [L^3T^{-1}]is the surface water flux between cells from the previous time step, g [LT^{-2}] is acceleration due to gravity, n [-] is Manning's roughness coefficient (see Arcement and Schneider, 1989), h [L] is nodal water depth, z [L] is elevation, h_{flow} [L] is the water depth difference between adjacent cells, x [L] is the grid cell width and t [T] is time. Having established the discharge across all four boundaries of a cell, the cell water depth (h) is updated using Eq. (7), where i and j are cell co-ordinates.

$$\frac{\Delta h^{i,j}}{\Delta t} = \frac{Qsw_x^{i-1,j} - Qsw_x^{i,j} + Qsw_y^{i,j-1} - Qsw_y^{i,j}}{\Delta x^2} \tag{7}$$

To maintain stability, the Lisflood component calculates the maximum allowable length of the next time step (Δt_{max}) for which a converging solution is highly likely to be maintained. The calculation is based on the shallow water Courant-Friedrich-Levy (CFL) condition, in which:

$$\Delta t_{\max} = \alpha \frac{\Delta x}{\sqrt{gh}} \tag{8}$$

The coefficient α is typically defined as being between 0.3 and 0.7 (Bates et al., 2010), and is used to enhance the model's robustness, as the CFL condition is a necessary but not sufficient condition for nonlinear systems. As Eq. (8) demonstrates, this is strongly influenced by the grid cell size and the water depth. A typical Δt_{max} for a 50 m grid spacing, an intermediate α and with surface water present is in the order of a minute.

Lisflood-FP has been extensively tested and benchmarked by Bates et al. (2010) and Neal et al. (2011), demonstrating that the model is capable of simulating flow depths and velocities within 10% of codes that solve the full two-dimensional shallow water equations.

2.1.3. Subsurface flow

Subsurface flow is simulated at the near-surface (saturated soil in Fig. 3) and deeper subsurface (groundwater in Fig. 3) using a two-dimensional lattice of square cells interacting according to the

von Neumann-type neighbourhood in a technique similar to that utilised by Rothman (1988). Both the near-surface and deeper subsurface components are similar conceptually and can pass water within and between themselves. The near-surface component represents an unconfined fully-saturated flow within the soil along the bedrock-soil interface, with the top of the bedrock defining the flow base. The deeper groundwater component is again unconfined, but flow is within the bedrock itself. Here the lower surface is at a predefined datum. The flow properties of the near- and deep-subsurface can be defined separately within the platform and both use the same algorithms to simulate flow. To ease model validation and sensitivity analysis (see Section 3), the near-surface component is not enabled in this study (potential recharge and baseflow are passed between the surface and deeper groundwater). However, its description is included for reference and it uses the same equations as the groundwater component described in this section.

Nodes representing groundwater consist of distributed, lateral, hydraulic conductivity, K [LT^{-1}], specific yield, Sy [−], and aquifer head (the unconfined potentiometric surface), h [L]. The difference in aquifer head between two adjacent cells drives inter-cell water flow. The governing equation for steady-state groundwater flow is defined by Bear (1979) as:

$$\nabla T \nabla h + W = 0, \tag{9}$$

where transmissivity, T [L^2T^{-1}], can be approximated by multiplying hydraulic conductivity by groundwater depth, and W [L^2T^{-1}] represents additional source and sink terms. From this, the one-dimensional, steady-state flow, Q_{gw} [L^2T^{-1}], may be defined as:

$$Q_{gw} = -T_s \frac{dh}{ds} \tag{10}$$

where, s is the coordinate aligned with flow direction. Integrating between two different groundwater heads (h_i and h_j) separated by a distance (we use Δx as it corresponds to the cell width in the flow direction x) yields:

$$Q_{gw} = \overline{T} \frac{h_i - h_j}{\Delta x} \tag{11}$$

Under a heterogeneous transmissivity, where abrupt changes may cause instability in the model, a flux limiting harmonic mean of the transmissivity for the two points i and j is used to calculate an averaged transmissivity, $\overline{T}$:

$$\overline{T} = \frac{2T_iT_j}{T_i + T_j} \tag{12}$$

The total flux to a central cell, Q^*_{gw} [L^3T^{-1}], is a combination of fluxes from the neighbouring cells (using Eq. (11) for the four adjacent cells as per the von Neumann scheme, see Fig. 1) and the additional source and sink term. Recharge from the surface hydrological component provides the source term and baseflow-return to the surface acts as a sink. Total fluxes are used to update groundwater heads at each point in the aquifer domain simultaneously at each time step (Δt) using the discrete mass balance equation:

$$h_{t+\Delta t} = h_t + \frac{1}{Sy} \frac{Q^*_{gw}}{\Delta x^2} \Delta t \tag{13}$$

Two user defined lateral groundwater boundary condition types have been implemented into the CLiDE platform. Specified (Dirichlet) boundary conditions fix aquifer head at the boundary and a no-flow (Neumann B) condition sets flux across the boundary to zero. The base of the aquifer is bound with a specified boundary allowing leakage, which is included in the flux algorithm as a secondary source or sink term. The surface boundary allows a flux of water to be returned to the surface component as baseflow where aquifer head is greater than surface water, r [L], for a particular node. The volume of water returned to rivers, q_{bf} [L^3T^{-1}], is dependent on the specific yield of the groundwater node and the thickness (RB_b [L^3]) and hydraulic conductivity (RB_k [LT^{-1}]) of the river bed using a modified version of the equation derived by Haitjema (1995):

$$q_{bf} = Sy\left(\frac{h - r}{c}\Delta x^2\right) \tag{14}$$

$$c = \frac{RB_b}{RB_k} \tag{15}$$

To ensure model stability when passing water laterally, the cell Reynolds number, Rn [-], is calculated at each node for each time step and a flag is raised if it exceeds unity. Reduction of the Reynolds number is possible by reducing the time step (undertaken automatically by the platform for the entire domain if a flag is raised for any particular cell) or increasing the cell size (this can be undertaken manually by adjusting the resolution of the input datasets). Roache (1976) defines the Reynolds number as:

$$Rn = 4\frac{T}{Sy}\frac{\Delta t}{(\Delta x)^2} \tag{16}$$

2.2. Sediment transport component

There are several sediment transport models that could be used to evaluate landscape evolution at the decadal to centennial timescales required for the CLiDE platform. Coulthard (2001) and Merrit et al. (2003) review these, and an overview of the theory behind modelling landscape evolution is presented by Tucker and Hancock (2010). The ability of current models to employ distributed fluvial and erosional processes is an advantage over previous approaches (see Kinnell, 2010). Current models are based on DEMs, include distributed soil depths, allow surface runoff, and can automatically determine inter-cell slope gradient and transport of sediment. For this study, CAESAR-Lisflood was selected to provide the sediment transport and Graphical User Interface (GUI) functionality for the CLiDE platform, as it has a modular, versatile design and has been verified in a range of environmental settings.

The ability of CAESAR/CAESAR-Lisflood to predict soil erosion has been tested against experimental field data for a small catchment (see Coulthard et al., 2012), where predicted suspended sediment and bedload yields showed a close correspondence in both volume and timing of field measured data. Due to its adaptable nature, CAESAR has been used for many applications including: modelling the response of river systems to environment change (Van De Wiel et al., 2011); human impact on fluvial regimes and fluxes of sediment (Hoffmann et al., 2010); influences of vegetation on river development (Tooth et al., 2008); catchment response to environmental change (Coulthard et al., 2005); and, more recently, determining catchment soil loss rates (Hancock et al., 2011). The remainder of this section describes the major features of CAESAR that have been built upon by CLiDE. See Coulthard and Van De Wiel (2006) and Coulthard et al. (2013) for further detail regarding the equations that drive sediment transport within CAESAR.

Using the water fluxes between cells from the surface hydraulic model (Eq. (6)), velocities in the x and y directions are calculated. The resultant velocities are then used to calculate a cell shear stress

that provides an input into a choice of two well established sediment transport laws: Wilcock and Crowe (Wilcock and Crowe, 2003) or Einstein-Brown (Einstein, 1950). These formulae are selected as they both calculate total sediment transport from the sum of individual grain size fractions, which is important for grain the sorting processes within the platform.

The Wilcock and Crowe method can transport sediment within a catchment as both a suspended load and a bedload. Both depend on the volume of sediment transported per time step, where the sediment transported from a central cell to a neighbouring cell is calculated by equating a coefficient to either slope, for bedload transport, or velocity, for suspended load transport. The calculation of suspended load transport is simplified, as it assumes an equal distribution of sediment throughout the water column. Sediment deposition also differs between the two transport types, with bedload sediment deposited (and subsequently re-entrained) at every time step, and suspended sediment deposition based on fall velocities. Under a quasi-uniform sediment grain-size regime, the computationally less expensive Einstein-Brown method for transport may be employed. The formulation evaluates the forces moving and restraining a particle. A bedload transport rate can be calculated from these forces and used to approximate the flux of sediment between cells. The amount of sediment that can be transported is calculated and moved from an active layer, which integrates sediment transport across the multiple grain-sizes (see Van De Wiel et al., 2007).

The incorporation of multiple grain-sizes, selective erosion, transport and deposition of the different size fractions is important and results in spatially variable sediment size distributions. Since this variability is expressed not only horizontally but also vertically, it requires a method of storing subsurface sediment data. This is carried out by using a system of layers comprising: the active layer representing the stream bed; multiple buried layers (strata); a base layer; and, if required, a non-erodible bedrock layer (Van De Wiel et al., 2007). It is worth noting that the size of an individual grain is not allowed to evolve during the simulation.

Non-fluvial sediment transport occurs through instantaneous debris flow and a slower creep process. Debris flow is computed using a two-dimensional sand-pile algorithm (Metha and Barker, 1994) based on a critical slope angle. Where this angle is exceeded, an iterative process, contained within a single time step, moves material down slope to lower cells until the critical angle is no longer exceeded. Soil creep is calculated using a gradient in elevation between cells on a monthly basis through a diffusion equation (Culling, 1960).

Vegetation cover in the model is implemented by specifying areas where vegetation covers the surface layer, which has the effect of binding sediment and reducing erodibility (see Murray and Paola, 2003). A simple alluvial vegetation growth model (see Coulthard and Van De Wiel, 2006) is included, allowing linear growth of vegetation over time if it is not submerged. When vegetation has grown beyond a specified limit it restricts fluvial erosion to a percentage of that for uncovered sediment (default value is 10%). If flow shear stress exceeds a threshold the vegetation can be removed, thus exposing the sediment below to unhindered erosion. If vegetation becomes covered by sediment it can re-grow through the sediment layer, re-stabilising it.

3. Verification and sensitivity analysis

3.1. Verification of the groundwater component

Bench-marking of the groundwater component was undertaken through comparison to steady-state and transient analytical solutions. To ensure correct functioning of the groundwater model it was subjected to tests similar to those described by Ravazzani et al. (2011). These tests were undertaken on a 2 km wide, square domain with 10 m cell spacing and groundwater parameters representing an unconfined aquifer with a hydraulic conductivity of 2.5 m d^{-1} and a specific yield of 0.1. Two tests allowed an assessment of steady-state and transient flow behaviour.

In the first test a steady-state solution of the subsurface model was compared to an analytical result by simulating the response of groundwater level to constant uniform recharge. Northern and southern boundaries were set to the no-flow condition and eastern and western boundaries to Dirichlet conditions, which represented fixed stage (constant elevation) streams at 22 m (west) and 16 m (east). Recharge was constant in time and space at 0.5 mm d^{-1} and an initial groundwater head of 16 m applied to all regions. The simulation ran until a steady-state solution was reached and a cross section (west to east) of groundwater levels compared to the analytical solution (see Harr, 1962). The simulated and analytical solution show excellent agreement (a root mean square error (RMSE) of below 0.01 m) after a couple of hundred iterations (Fig. 5).

The second stage of testing involved the simulation of groundwater head in response to a constant pumping rate and comparison to an analytical solution. A modified approximation of the Theis solution, valid for unconfined aquifers (Barry et al., 2000), was used with a small extraction depth to aquifer thickness ratio. Initial head was set at 50 m for all nodes, with a constant pumping rate of 150 m^3 d^{-1} from the central node and a time step of 360 s. Dirichlet

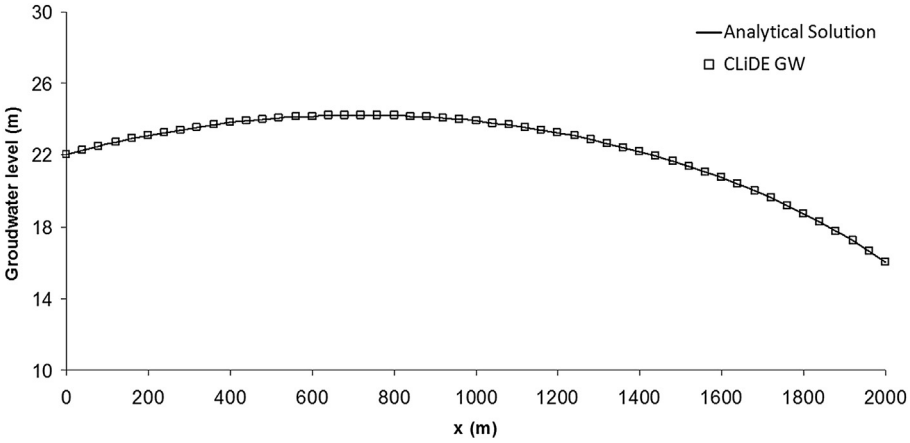

Fig. 5. Steady-state comparison of the groundwater component to an analytical solution for water table elevation between fixed streams under uniform recharge conditions.

boundary conditions were set to match the initial head along all lateral boundaries and groundwater levels monitored at four sites set at 50 m intervals between 100 m and 250 m from the well. The match between transient simulation and analytical solution is good, with close agreement at all well distances (Fig. 6).

3.2. Sensitivity analysis

By modifying the specific yield and hydraulic conductivity of the subsurface, the groundwater residence times and groundwater storage volume are changed, and subsequently the baseflow-returns to surface flow are perturbed. A numerical experiment was devised to test the sensitivity of baseflow-return and sediment transport within an idealised catchment to differing groundwater regimes with identical boundary conditions (rainfall, potential evapotranspiration and initial topography). Analysis of the sensitivity allows impacts of the differing groundwater regimes to be assessed for a simple catchment.

3.2.1. Platform setup

To keep topographic effects to a minimum a catchment with simple topology of a gentle V shaped valley, as per Coulthard and Van De Wiel (2006), was created (Fig. 7). A cell width of 10 m was selected, allowing a reasonable simulation time (approximately 3 days per simulation for a standard desktop with an octa-core processor) whilst maintaining stability in the groundwater model: a higher spatial resolution would require shorter time stepping (see Eq. (16)).

A total of 0.1 m rainfall was applied uniformly over the catchment for the first hour of each day during each of the 3600 days of simulation. Potential evapotranspiration was set to 0.01 m d^{-1} for the duration of each simulation. Land use and soil type, which determine the partitioning of soil water in the SLIM module (see Section 2.1.1.), were fixed and representative of arable land sitting on an unconsolidated, macroporous soil with little by-pass flow (see Boorman et al., 1995). Sediment grainsize was 4 mm across the catchment and all sediment transport treated as bedload.

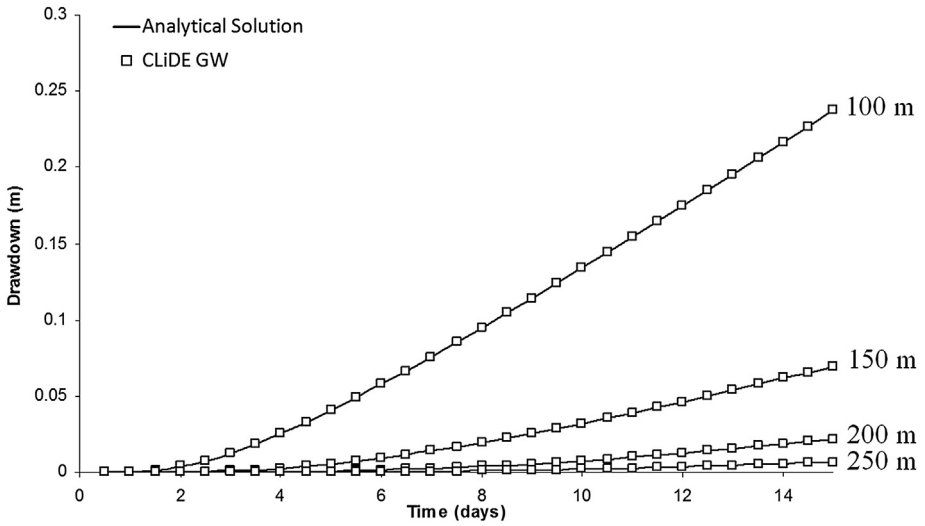

Fig. 6. Comparison of drawdown calculated by the modified Theis solution and the groundwater component of CLiDE. Distance of each location from the pumping site is given at the right of the graph.

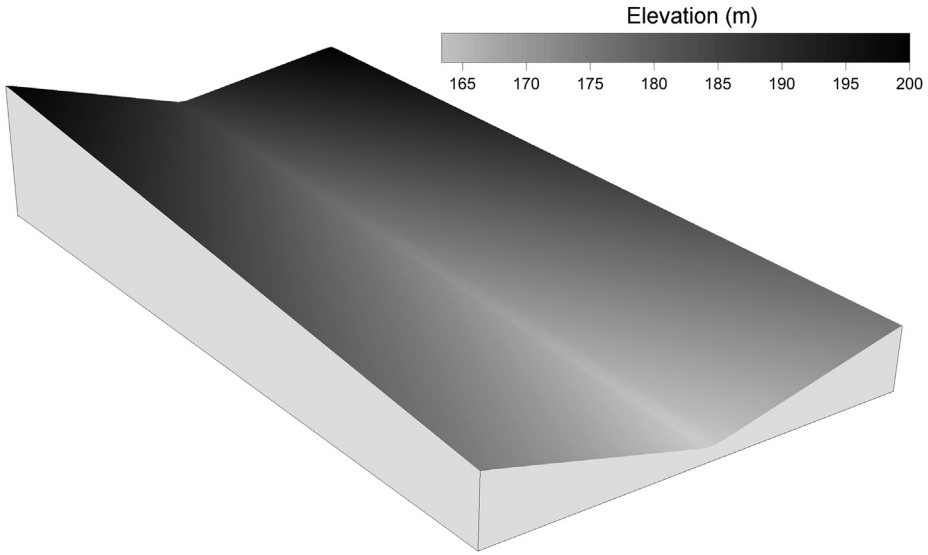

Fig. 7. Simple catchment used for the sensitivity simulations. The catchment is 125 by 250 nodes at 10 m grid spacing.

Table 1
The groundwater conditions for each of the 7 scenarios simulated for the test catchment.

Run number (scenario)	Groundwater recharge from surface?	Baseflow-return to surface?	Specific yield (−)	Hydraulic conductivity (m d^{-1})
0	Yes	Yes	0.1	1
1	Yes	No	–	–
2	No	No	–	–
3	Yes	Yes	0.1	100
4	Yes	Yes	0.1	0.001
5	Yes	Yes	0.5	1
6	Yes	Yes	0.005	1

To assess the changes in water and sediment fluxes, seven scenarios with differing hydrological characteristics were created (see Table 1). Scenario 0 allows both recharge and baseflow-return with specific yield and hydraulic conductivity set at intermediate values. Scenario 1 simulates recharge from the surface to groundwater, but has no baseflow-return component. This is representative of a deep, unconfined water table. Scenario 2 is representative of an impermeable surface, not allowing recharge or baseflow-return. The remainder of simulations (scenarios 3 to 6) allow both recharge and baseflow-return with differing specific yield and hydraulic conductivity. For all scenarios groundwater boundaries were set to the no-flow condition. Groundwater levels and baseflow-return were monitored across the catchment, while sediment yield and fluvial flow were recorded at the outflow point at the base of the catchment.

3.2.2. *Hydrological characteristics*

The groundwater properties in scenario 0 represent an unconsolidated silt, which produces a relatively stable daily groundwater head under the simulated fluctuating surface hydrological conditions. The result is a permanent river flow at the base of the catchment. Over the length (temporal) of the simulation river flow increases and groundwater heads decrease. The lower areas of the catchment are provided with water for longer periods than they would receive solely through runoff during rainfall events. Scenario 1 represents a deep groundwater table with no baseflow-return to the surface. Here, water can still be stored at the surface as soil moisture, but no water is transported back from the subsurface, creating an ephemeral river, which disappears shortly after the daily rainfall episode ceases. This scenario produces the lowest daily river discharges as water is not returned to the surface as baseflow. Scenario 2 is representative of an impermeable surface that does not allow the transfer of water between the surface and subsurface. Under these conditions all water is either transported across the surface, stored at the surface as soil moisture (with no lateral or horizontal flow), or removed through evapotranspiration.

Scenario 3 uses a high hydraulic conductivity, resulting in a much quicker flow of water within the subsurface compared to the baseline (scenario 0). There is an initial flux of water from the ground to the surface, as groundwater heads adjust themselves to a new equilibrium position from the initial conditions (see Fig. 8). As incision of the central channel progresses, further water is released from the subsurface store to the river as the groundwater levels seek a new equilibrium position within the altered landscape. The low hydraulic conductivity in scenario 4 reduces groundwater flow (when compared to scenario 0) and, as there is sufficient rainfall, creates groundwater levels that are highly dependent on local surface elevation. This is apparent in Fig. 8, where groundwater volumes across the catchment increase from their initial starting point up to the local surface elevation over the first 200 days of simulation. Although a central channel is created during the simulation, groundwater levels at any particular point reflect local surface contours. Therefore, only a minimal amount of water is released from the groundwater store, resulting in a gradual loss of water from 300 days onwards in the simulation (Fig. 8).

The comparatively high specific yields in scenario 5 create a stable groundwater level that is highly influenced by the lowest elevation in the catchment. Recharge is not sufficient to maintain groundwater heads as subsurface water is lost to the river as baseflow. As there is a relatively large volume of water held in the aquifer, channel incision has the potential to release a large amount of water from the subsurface to the surface. This is due to incision

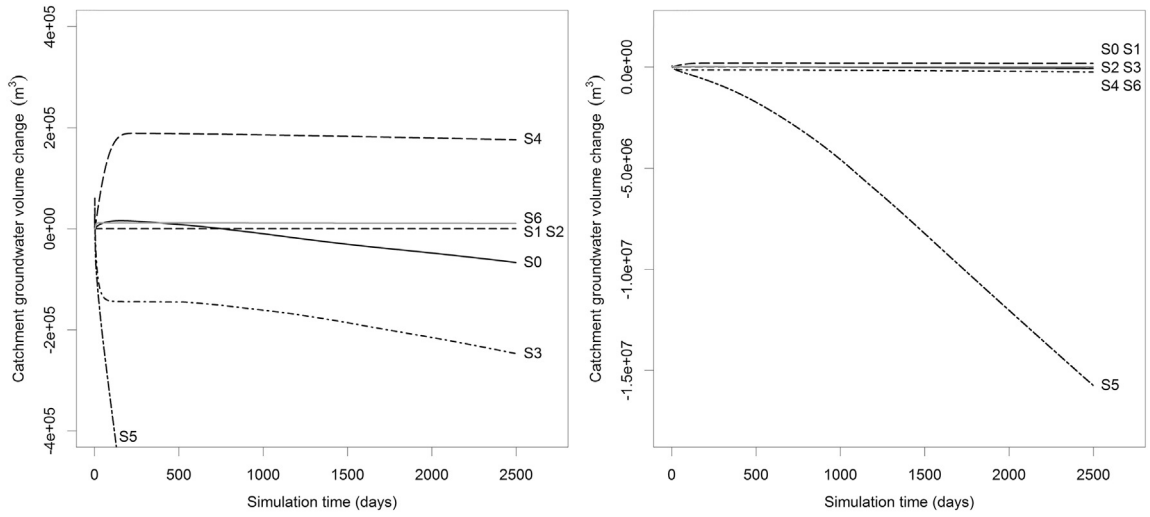

Fig. 8. Simulated change in catchment groundwater volumes following initialisation. Negative gradients represent a loss of groundwater to the surface as baseflow-return. The left and right plots show the same data, with differing vertical (groundwater) scales.

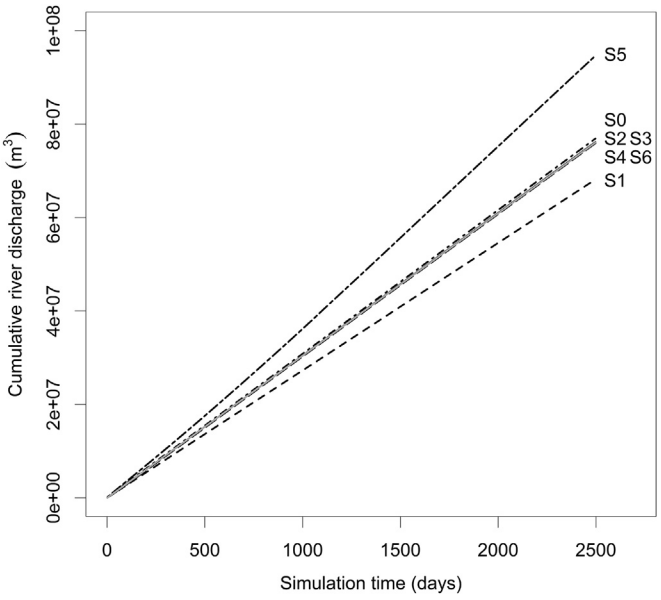

Fig. 9. Cumulative river discharge at the catchment outlet.

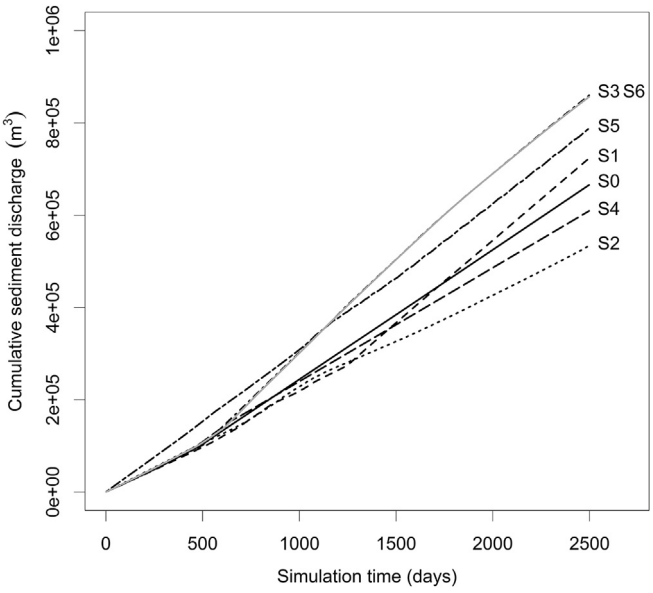

Fig. 10. Cumulative sediment yield at the catchment outlet.

along the channel length lowering the water table and introducing water from the groundwater store to the surface, leading to an increase in river discharge (see Fig. 9) and a large drop in groundwater volume (see Fig. 8). Low specific yields create highly variable groundwater levels with a dependency on recharge rates. Assuming no flow in or out of a node, the specific yield used in scenario 6 produces a 1 m rise in groundwater levels for every 5 mm of recharge. As there is adequate rainfall, groundwater levels sit at the ground surface across the catchment during rainfall events and excess water is routed across the surface. During the intervening periods, hydraulic conductivity is not sufficient for groundwater levels to recede. As the overall volume of water contained in the aquifer is low, the carving of the central channel does not release a significant amount of water from the ground for contribution as river baseflow.

3.2.3. *Sediment transport*

Cumulative sediment discharge is presented in Fig. 10. Initially scenario 5 (high baseflow contribution) creates the highest rate of sediment discharge, however after 500 days of simulation scenarios 3 (flashy baseflow) and 6 (low baseflow) create the highest rate of daily sediment discharge. Scenario 1 (no baseflow) initially has the lowest sediment discharge, however a switch in behaviour after 1250 days increases sediment discharge rates similar to those exhibited by scenarios 3 and 6. Catchment sediment discharge for the intermediate groundwater, impermeable surface and low hydraulic conductivity scenarios (0, 2 and 4 respectively) produce quasi-linear rates of catchment sediment discharge without experiencing the same marked change in rates experienced during the other scenarios.

There do not appear to be any clear relationships between daily river discharge and sediment discharge when the scenarios are assessed cumulatively. When river and sediment discharge are plotted against each other through time (Fig. 11 and Fig. 12) some clear trends begin to emerge. For each scenario the changes in sediment discharge rate are not constant with respect to time, but instead are held for a number of years before abruptly transitioning to the next discharge rate. The small range in river discharge values throughout each simulation highlights these horizons, by producing a banding of the data with interspersed points in Fig. 11 and Fig 12. A similar behaviour is exhibited in all scenarios (excluding scenario 5), albeit with differences in the sediment discharge rates and the time held at a particular value.

The intermediate groundwater scenario (scenario 0, Fig. 11) initially outputs 200 $m^3\ d^{-1}$ sediment discharge for around 500 days, and then quickly establishes a new catchment sediment discharge rate of 280 $m^3\ d^{-1}$, which it maintains until the end of the simulation. This behaviour is similar to that exhibited by scenario 4 (Fig. 12). The scenarios producing the highest rates of sediment discharge (3 and 6) have the same temporal sediment-river discharge signature. As these simulations progress, sediment discharge increases from 200 $m^3\ d^{-1}$ up to peak of around 425–450 $m^3\ d^{-1}$ at around 500 days into the simulation. Sediment

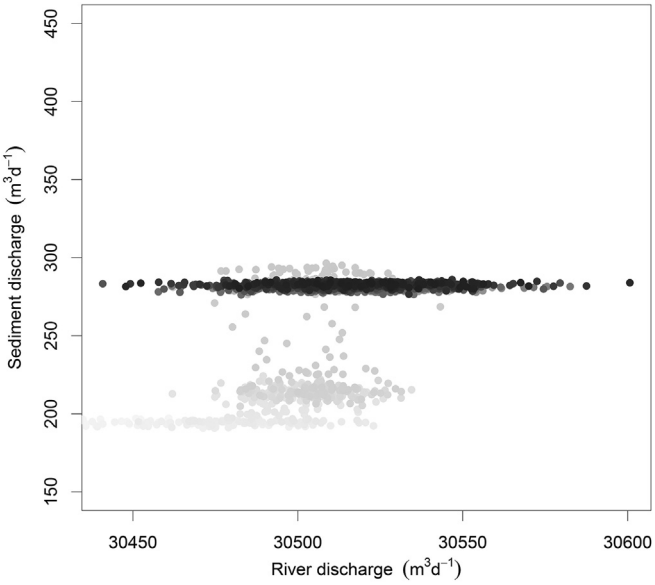

Fig. 11. Catchment daily sediment discharge plotted against daily river discharge for the intermediate groundwater scenario (scenario 0). The greyscale of points represents the position in time within the simulation (black at the end of the simulation and light grey at the start).

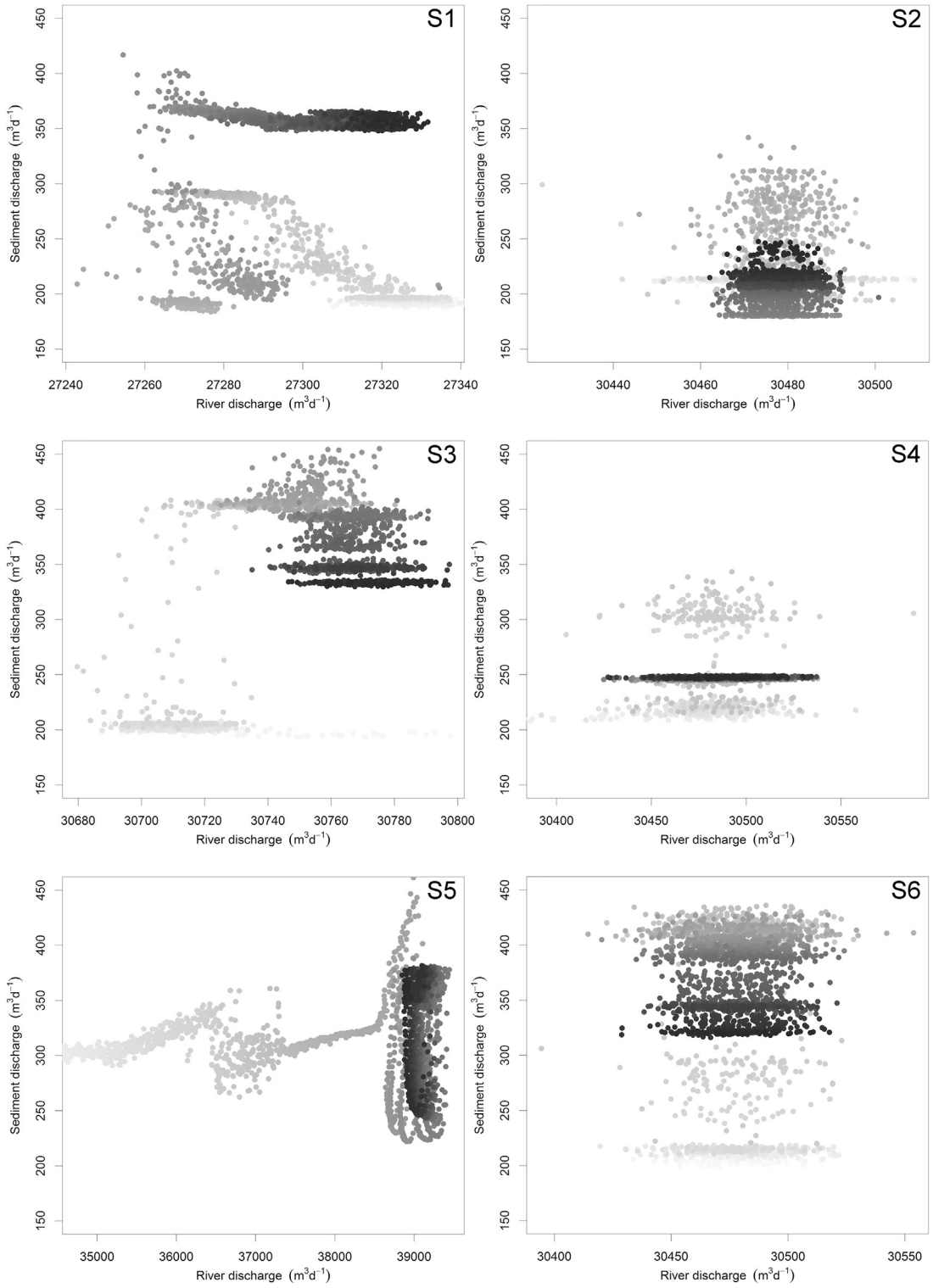

Fig. 12. Catchment daily sediment discharge plotted against daily river discharge for each groundwater scenario (numbered in top right of each plot). The greyscale of points represents the position in time within the simulation (black at the end of the simulation and light grey at the start). The same scale is used for sediment discharge, however the river discharge scale is variable.

discharge then drops slowly, to around 325 $m^3\ d^{-1}$ where it remains until the end of the run. Scenario 5 (high baseflow) is the only setup where a significant change in daily river discharge occurs, increasing by 5000 $m^3\ d^{-1}$ over the simulation. Despite both not having a groundwater input, scenarios 1 and 2 exhibit markedly differing temporal sediment-river discharge signatures. Scenario 2 (no losses to recharge) has a relatively uniform daily river discharge, with sediment discharge initially starting at 200 $m^3\ d^{-1}$, rising for a short period to 300 $m^3\ d^{-1}$ before falling back to its initial rate. Scenario 1 (losses to recharge) has a river discharge that changes as the simulation progresses, producing horizons of sediment transport at differing points in time and river

discharge. The end of this scenario exhibits the highest sustained rate of discharge from the catchment, despite the lowest river discharge rates.

Comparison of the temporal sediment-river discharge signatures (Fig. 11 and Fig. 12) confirms that there is no overarching relationship that can be defined for river and sediment discharge at the catchment outlet. They highlight the finer details of the sediment discharge rates through time, in particular their propensity to remain at a steady-state sediment discharge for a period of time before abruptly moving to a differing steady-state discharge rate. These changes represent differing internal morphological dynamics occurring within the catchment itself. Differences between the scenarios are formed by the feedbacks that individual hydrological characteristics create with their surrounding morphology. Morphology is initially the same for all scenarios. However, following initialisation each hydrological scenario creates unique distribution of fluvial flow velocities along the river reach, each producing a different value for sediment transport and hence erosion characteristics. Once a morphological feature is well-enough defined for a particular cell, it will start to have an impact on the surrounding cell fluvial characteristics. This feedback can in some cases create rapid changes in morphology between steady-states. For example, a depression forming in the channel at the base of the catchment can accelerate flow velocities immediately upstream, leading to their erosion to the same depth as the initial depression. This process can rapidly cascade upstream until there is insufficient water available to continue the process (the river reach does not extend to the top of the catchment in these scenarios). In the majority of the sensitivity analyses scenarios this process leads to rapid incision of the main channel from the base of the catchment after 500 days of simulation, creating the inflection in sediment discharge responses (see Fig. 10). It is also responsible for the move away from the initial steady-state (lightest grey horizons in Fig. 11 and Fig. 12) to subsequent steady-states in the sediment-river discharge plots. Exceptions to this were scenario 1, where the main channel incised after 1,250 days, and scenario 5, where incision occurs immediately after initialisation.

3.2.4. Conclusions

Modification of the system hydrology, by means of changing the surface or subsurface properties, creates a range of river discharge responses at the catchment outlet. Sediment discharge at the outlet is not a function of daily river discharge, but transitions through a series of steady-state values independently of the daily river discharge value. This behaviour is controlled by the internal morphological dynamics generated from the feedbacks between localised peak fluvial velocities and the evolving channel morphology.

At the catchment scale, evolving morphology can have an impact on the hydrological processes. This is particularly evident when the channel incises and the drop in river stage reduces surrounding groundwater heads (see Fig. 8, scenario 5) and increases river discharge (see Fig. 9, scenario 5). These effects would be strongest for a scenario with high specific yields and hydraulic conductivities, which would make a large volume of water available for baseflow return as the channel incises and groundwater heads fall over a large area without much time-lag.

Given that the morphology of a simple catchment can evolve in a variety ways based on local hydrological conditions, an accurate representation of baseflow-return influences on regional scale landscape evolution for a groundwater dominated catchment may be essential. To test this hypothesis we assess the impact of baseflow-return on shaping the morphology of a test catchment, the upper Eden Valley, UK.

4. Sediment transport in the upper Eden Valley

The role of groundwater in shaping catchment-scale surface geomorphology in the upper Eden Valley, a region where baseflow is a major contributor to surface water, is examined. Two scenarios were simulated: with- and without-groundwater recharge and baseflow-return. Aside from this, both have identical initial conditions and external forcings. For the without-groundwater scenario the groundwater module is not enabled. Therefore, baseflow-return is non-existent and all excess water (see Fig. 4) is available at the surface for routing as runoff (equivalent to scenario 2 in Section 3.2). As baseflow is no longer contributing to the surface hydrology, there will be less fluvial flow between rainfall events. As recharge is no longer removed during rainfall events, there is a potential for a higher fluvial flow rate. However, there is also no baseflow-return during these events so the difference in surface peak flow between the two scenarios should be dependent on the previous rainfall history and the hydrogeological characteristics. For both scenarios, the basin sediment yield and DEMs showing morphological changes are recorded. This allows an evaluation of the impact of groundwater on the geomorphology of the basin.

4.1. Case study

The Eden catchment, located in north-west England, is an upland area of 2288 km^2 (see Fig. 13). The Eden Valley sits between the Lake District National Park to the west, and the Pennines, a range of hills which divide North West and North East England, to the east. The most steeply elevated sections of the catchment are located on the eastern side of the valley, whilst the western side is flatter. The land mainly consists of pasture and is considered an important study area due to its water resources (Fowler et al., 2007), significant biodiversity and recent history of large-scale flooding events (Malby et al., 2007). Rainfall in the Eden Valley is above the UK annual average, with approximately 1000 mm y^{-1} on low-lying areas and 1500 mm y^{-1} on the higher ground (Daily et al., 2006). The major river within the region is the River Eden, which runs from the Pennines to the Solway Firth estuary, at the border between Scotland and England.

The study area is set in the upper part of the Eden catchment, above Temple Sowerby, an area covering 615 km^2. The Eden tributary has three gauging stations along its reach. Due to their positions relative to the model boundary, only the Temple Sowerby station allows calibration to gauged river flow data.

Catchment geology is composed of sedimentary units deposited between 450 and 220 million years ago, with central valley sections consisting of Permo-Triassic sandstones, and the surrounding upland of Carboniferous limestone (Fig. 13). Two major aquifers are contained in the Permo-Triassic sandstone formations, separated by the Eden Shale Formation. The Penrith Sandstone Formation (early Permian), which supplies large quantities of groundwater for public use through a series of boreholes, is confined to the east by the shale formation and to the west by drift cover. Parts of the Penrith Sandstone Formation are silicified, having a significant effect on the subsurface flow characteristics, with mean hydraulic conductivity of 0.8 m d^{-1} (Allen et al., 1997). Upper sections of the St Bees Sandstone Formation (early mid-Triassic) are also considered to be of hydrological importance, with mean hydraulic conductivity of 0.24 m d^{-1} (Allen et al., 1997). The surrounding Carboniferous Limestone Formation is also significant in this study area as it provides baseflow-return to streams in the sub-catchments of the upper Eden Valley and generates springs along the western margins (Mayes et al., 2006). The sandstones that run down the centre of the Eden catchment were eroded into a valley before the last glaciation. Subsequently, glacial processes formed

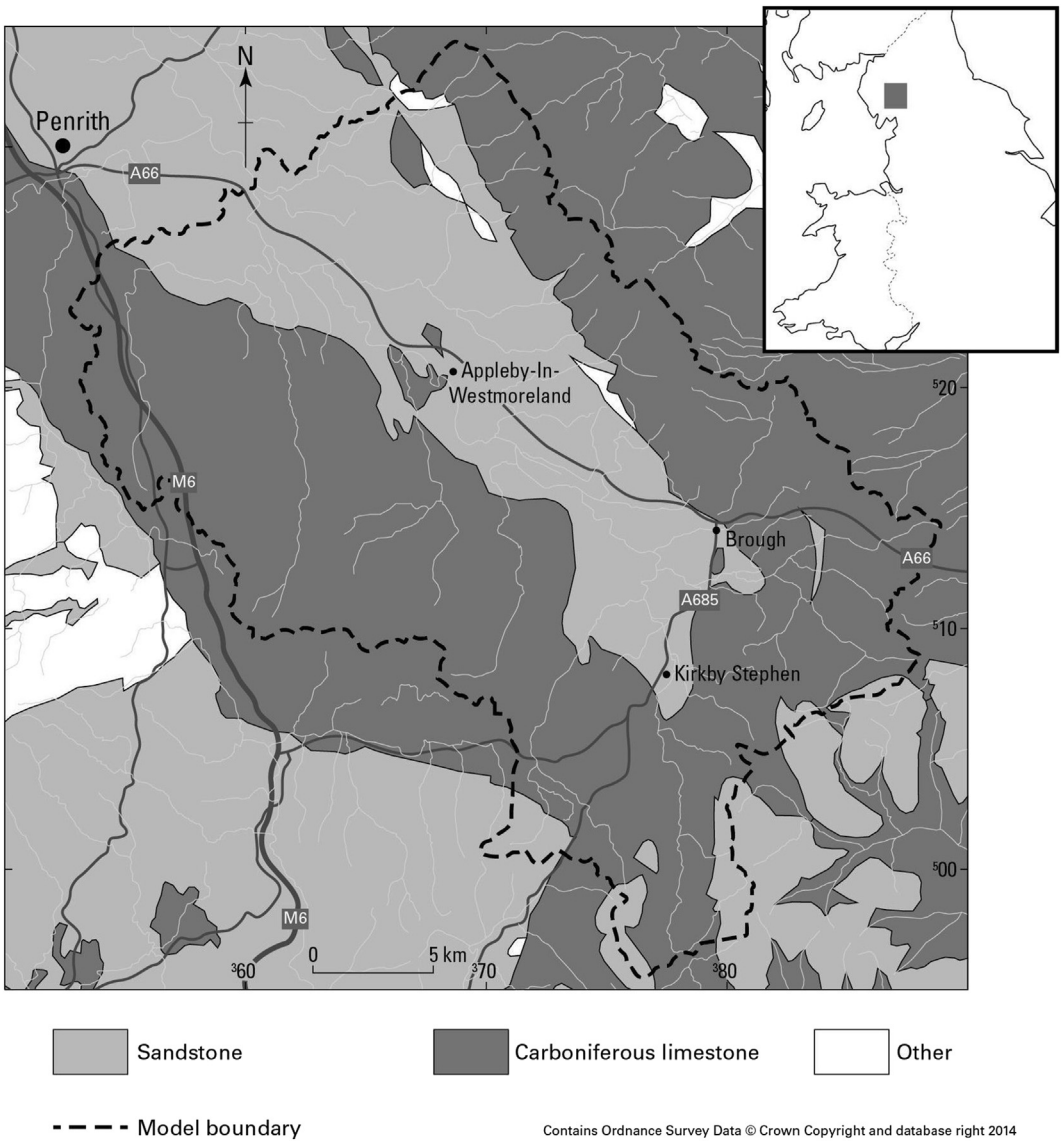

Fig. 13. Map showing the location of the upper Eden Valley study site within the north of England (insert) and a geological map of the catchment and model domain (main).

drumlins and, in some areas, scoured hollows into small basin features.

Due to the shallow depth of the water table in lowland areas, groundwater flow in the upper Eden Valley is dominated by discharge to the River Eden (Butcher et al., 2006; Bennett et al., 2003), with contributions from the subsurface along the majority of its length. Groundwater levels in upland regions of the study area may be up to 100 m the below surface. However, groundwater recharge in these regions drives subsurface flow and discharge rates in the valleys below. For a detailed review of the baseflow-return mechanisms, the reader is directed to Payn et al. (2012), whose study provides and assesses the spatio-temporal relationships during a seasonal baseflow recession.

4.2. Implementation

Initial setup of the upper Eden Valley model requires a calibration of the input parameters through a matching of simulated and observed data. Here we provide a comparison of the calibrated model to observed data. A detailed description of the calibration process, which involves modifying the baseflow index and rooting depth characteristics for surface flows and the hydraulic conductivity and specific yield for groundwater flows, is provided by Barkwith and Coulthard (2014).

The model calculates on a daily time step: the terrain elevation (metres above sea level (masl)), groundwater level (masl), baseflow (m^3), near surface storage (m^3), groundwater recharge (m^3), soil moisture deficit (m) and surface water flow (m^3). To assess the errors associated with differing water flow routes, and to simplify the process, time-series of simulated groundwater and surface flow are calibrated to observed data separately. Comparison of the surface hydrological flows to a baseflow separated record from the Temple Sowerby gauging station is shown in Fig. 14, with the differences between measured and simulated data overlaid. It is important to note that although the RMSE (calculated as 0.03 Ml d^{-1}) of the modelled and measured data suggests a good agreement, the peak differences do not take time-lag errors into account and therefore small temporal errors can create seemingly large differences between simulated and measured datasets.

Following calibration of the surface routed water, based on reducing RMSE (taking into account the full length of the

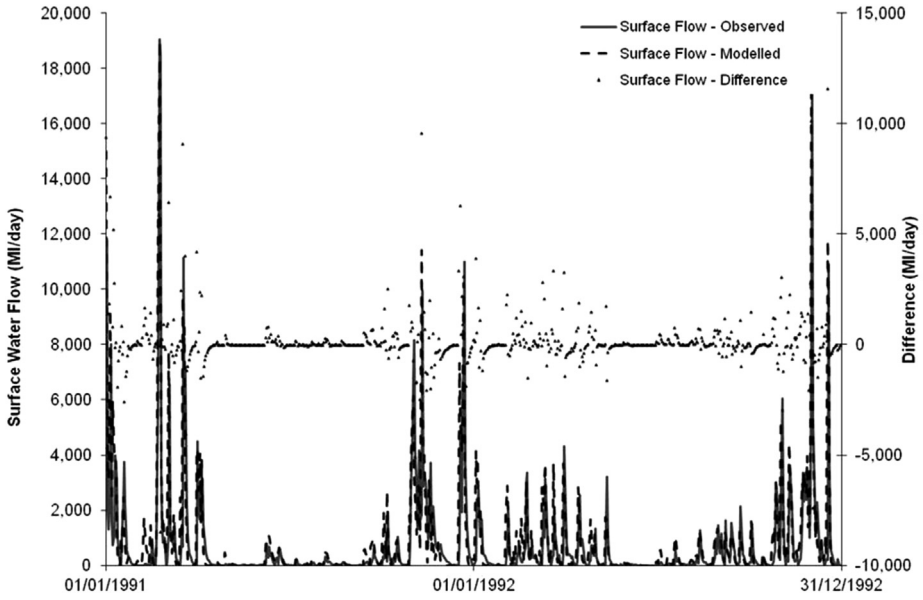

Fig. 14. Modelled and observed river hydrograph for Temple Sowerby gauging station, Eden Valley catchment (1991–1992).

simulation) and assessment through an observed fitting process, groundwater levels are calibrated using a two-step iterative approach. The model is run with a temporally averaged recharge value until steady-state is achieved, followed by a two-year (1991–1992) transient simulation. Simulated groundwater levels are compared to observed groundwater levels and, where needed, modifications made to the hydraulic conductivity and specific yield, and the process repeated. The post calibration simulated and observed groundwater levels for the Great Musgrave borehole are shown in Fig. 15, with an associated RMSE of 0.27 m. Although the range of measured groundwater levels and recession rates are not well replicated by the model, the position of events and minimum groundwater levels exhibit good correspondence to the observed data. The disparity between simulated and observed groundwater levels arises from the simplistic nature of the conceptual model that underlies the groundwater simulation process. In reality the subsurface hydrology of the upper Eden Valley is a complex, heterogeneous system that is difficult to replicate in time and space using a simplistic approach. However, by including even a relatively poor representation of groundwater, the CLiDE platform achieves a closer conceptual match to the environmental system we are simulating. Using the current setup, and through further calibration and refinement of specific yield and hydraulic conductivity distribution from field data, a reduction in simulated groundwater level errors is expected to be possible. For present purposes, however, the disparity between measured and modelled results during the calibration phase is deemed to be acceptable.

With calibration complete, the model is setup to run over a two-year period (1991–1992) using daily rainfall and potential evapotranspiration. A 50 m grid spacing was used for the model spatial

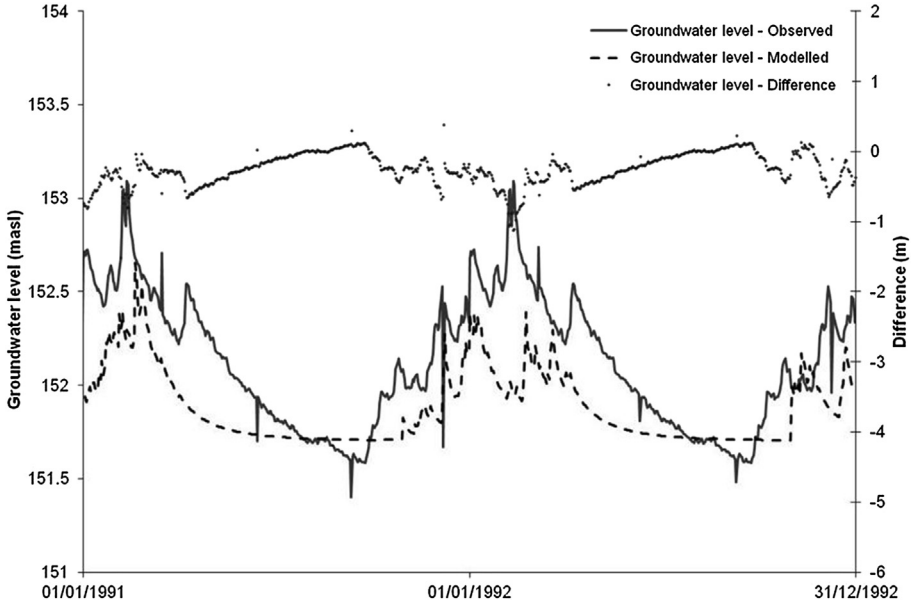

Fig. 15. Simulated and observed groundwater levels for the Great Musgrave borehole, Eden Valley catchment (1991–1992).

discretisation, and time stepping limited to between 1 and 3600 s for the sediment and surface fluvial transport processes.

4.3. Output and analysis

Time-series of sediment discharges from the catchment are presented for both with- and without-groundwater scenarios in Fig. 16. Initially sediment discharge in both scenarios increases rapidly as the sediment transport component progresses through the spin-up stage (first 5 months, where the model is allowed to reach a dynamic hydrological equilibrium). Significant sediment discharge events only occur during the larger rainfall events. However, as with the sensitivity analysis (Section 3.2), the amount of sediment transported from the system is not proportional to the amount of rainfall. For the majority of the simulation period the volume of sediment discharged is similar for the two scenarios, although they exhibit a differing temporal pattern of sediment flux, which is highlighted later in Fig. 18.

From the end of the spin-up period to the end of the simulation (a period of 19 months), the scenario including groundwater discharges a total of ~1800 m^3 more sediment from the catchment. During this period the greatest sediment transport event for both scenarios occurs on December 1st 1992, where a high rainfall event (47 mm) occurs on the previous day. Sediment discharge over this day increased from near zero in both cases, up to 25,803 m^3 for the groundwater scenario and 24,537 m^3 for the runoff only simulation.

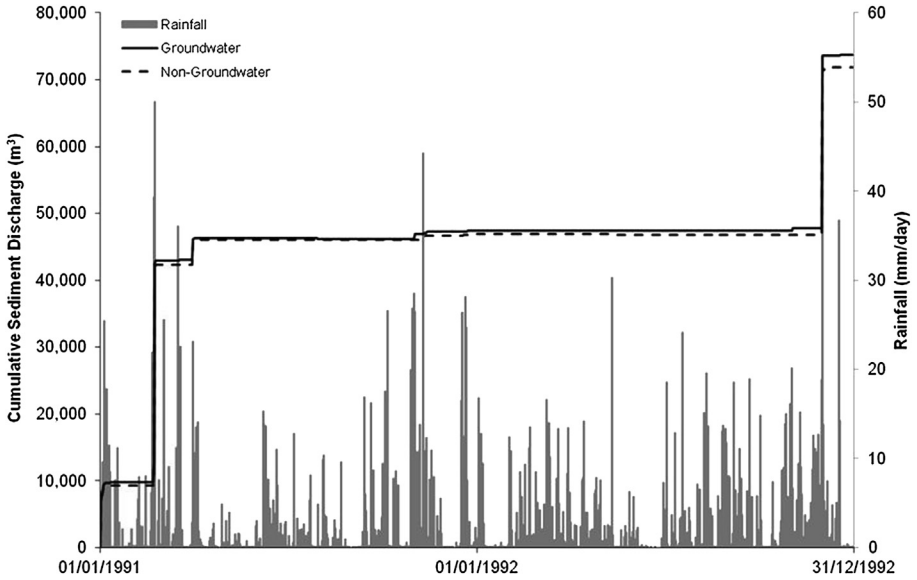

Fig. 16. Cumulative sediment discharged from the catchment for the with- and without-groundwater scenarios, and the catchment average rainfall over a two-year period.

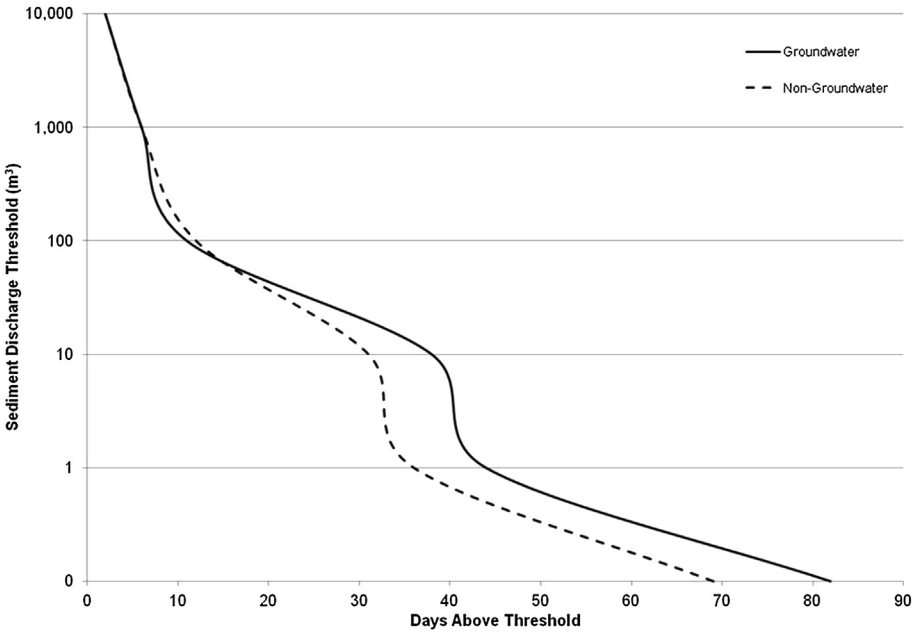

Fig. 17. The total number of days when daily sediment flux from the catchment exceeds a particular threshold value. As expected there are fewer days where over 1000 m^3 are discharged from the catchment compared to days where over 1 m^3 is discharged.

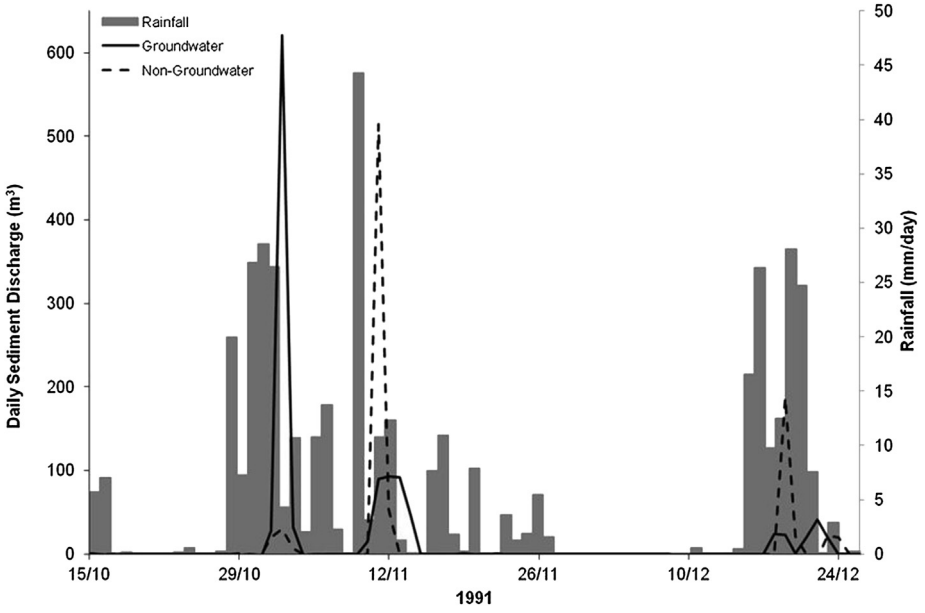

Fig. 18. Daily sediment discharge for the with- and without-groundwater scenarios overlaying average catchment rainfall between mid-October and the end of December 1991.

It is apparent from the cumulative plot that there are large periods of near zero sediment discharge throughout both simulations, where surface water velocity is not sufficient to transport sediment from the catchment. The total number of days when sediment flux from the catchment exceeds a particular threshold value is plotted for both scenarios (Fig. 17). Both scenarios produce the same number of days with sediment discharge above 1000 m^3. The scenario without groundwater has a few more days with an intermediate sediment discharge (between 100 and 1000 m^3). There are significantly more days where the groundwater inclusive scenario has a sediment discharge of between 0 and 100 m^3. These differences suggest that for this catchment groundwater is responsible for removing low, daily volumes of sediment over long periods of time.

Focussing on a few rainfall events over a short period allows a better descriptive analysis of the difference in the two scenarios. Fig. 18 includes daily sediment discharge for both scenarios and total catchment rainfall between mid-October and the end of December 1991. Sediment discharge events are initiated at similar times, but the groundwater inclusive scenario produces sediment transport over longer periods. During short, intense rainfall events, the without-groundwater scenario often produces a higher sediment discharge value than the subsurface flow inclusive scenario. The difference arises because a certain amount of water is routed to the subsurface store in the groundwater scenario, reducing overland flow and lowering the capacity to move sediment. However, this pattern can be reversed when a series of subsequent rainfall events, or persistent low intensity rainfall events, occur. Under these conditions, the system with baseflow-return transports increased volumes of sediment. The increase in sediment flux occurs where high baseflow levels from previous rainfall events increases total river flow above the threshold required to transport sediment. With groundwater included, this allows rainfall events that are not in themselves large enough to move sediment, to transport sediment with the added water provided by baseflow.

Fluvial channel, cell-averaged sediment flux (post spin-up) is plotted against altitude to assess the overall sediment transport dynamics within the catchment (Fig. 19). Small-scale oscillations (with a wavelength <50 m altitude) represent sediment that has been transported only short distances, creating erosion in the local upper nodes and accretion in the lower nodes. The short transport distances can be attributed to the movement of larger grain sizes that need sustained, high fluvial-velocities to travel long distances. Over the two-year period there is insufficient time for transport of these larger grains further than 50 m.

The difference between the with- and without-groundwater scenarios is not apparent at higher altitudes as the groundwater levels are well below the terrain surface and baseflow does not discharge into the rivers. Between 550 m and 450 m the effects of groundwater become apparent, increasing the peaks of erosion and deposition as surface flow velocities and sediment fluxes are increased. At lower catchment elevations the difference in the amount of sediment transported is diminished due to an overall reduction in slope inclination and river flow velocities.

Using a central moving average over several tens of metres in the up- and down-slope directions, the small-scale oscillations can be removed (example in Fig. 19 for the groundwater inclusive scenario only), revealing a large-scale pattern of increasing erosion from 650 m down to 350 m followed by a reduction in the erosion and deposition at lower altitudes. This large-scale change in the erosional response with altitude is likely to be topographically controlled for upper Eden Valley, as mid to high elevations are associated with increased topographic gradient in comparison to the lower reaches. Above 650 m, surface flow is not concentrated enough to produce sufficient volumes of water to transport sediment. At between 650 m and 350 m surface flow has begun to concentrate into streams and slope is sufficiently steep to favour surface runoff, with velocities great enough to entrain and transport sediment. At between 350 m and 200 m water is further concentrated and steam volumes are increased. However, topographic gradient is no longer sufficient to entrain sediment at the same rates as at higher altitudes (with steeper slopes) and the volume of eroded sediment is reduced with decreasing elevation. Below 200 m, surface flow velocities are diminished to the point where the volume of sediment entrained is smaller than that deposited, and accretion occurs.

Significant sediment discharge events only occur during periods

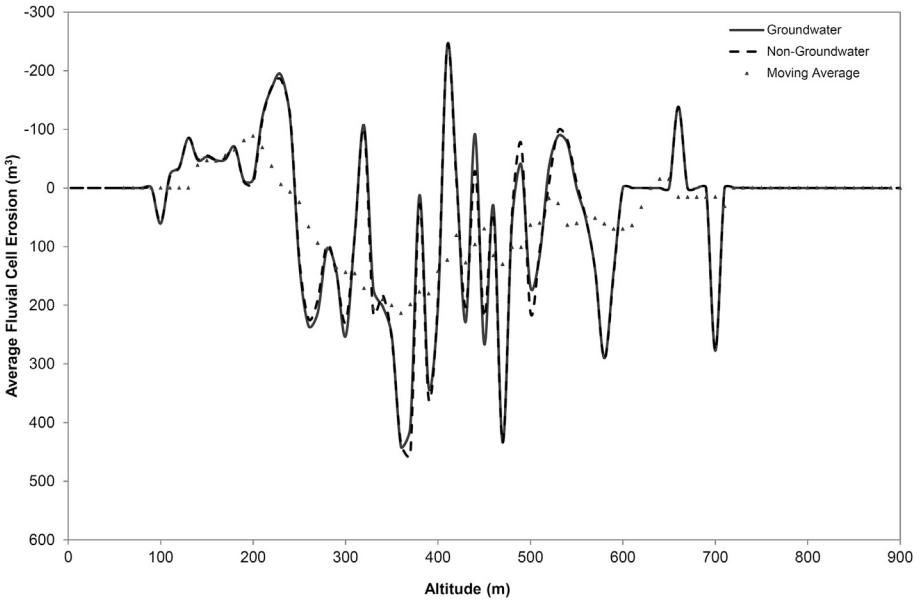

Fig. 19. Simulated erosion (or accretion) for fluvial cells averaged across bins of 10 m altitude. The plot highlights differences in erosion characteristics for the with- and without-groundwater scenarios and the larger scale pattern of erosion and accretion within the catchment after two-years of simulation. The moving average is shown for the groundwater inclusive scenario to highlight the larger scale trends.

of above average rainfall. As shown by Coulthard et al. (2012) and the sensitivity analysis (Section 3.2), the amount of sediment transported from the system is not necessarily proportional to the amount of rainfall. The same is true for this catchment. Although small, the difference that arises in the total sediment transported under the with- and without-groundwater scenarios is a result of the baseflow sustaining river water fluxes above the sediment pick-up threshold for greater time periods after high rainfall events. The timing of sediment transport events is not equivalent in the two scenarios. The runoff-only simulation exhibits a short-term flashy sediment discharge in response to intense rainfall events, whilst the inclusion of groundwater smooths the sediment discharge and introduces a 'memory' of previous rainfall events into the system. The large-scale trend of increased erosion at mid-elevations is due to the increased fluvial velocities that exist in these regions, and is largely controlled by topographic gradient. These trends are also likely to be, in part, due to the spatially differing distributed catchment surface water inputs.

5. Discussion

The following discussion covers an assessment of the modelling platform and calibration process, followed by the findings of the sensitivity test and an outline of the impact that groundwater has on the upper Eden Valley geomorphology, with a focus on the traits that may be applicable to other catchments. The final section discusses caveats and uncertainties associated with the platform and modelling process.

5.1. Platform assessment

A modelling platform has been created that has the potential to simulate a range of environmental systems. The CLiDE platform was constructed using existing landscape evolution algorithms for the transport of sediment and surface hydrodynamics. These were driven by a new method for the partitioning of water into evapotranspiration, surface, soil and groundwater stores, which was coupled to groundwater flow algorithms via recharge and baseflow-return. Assessment of the new platform was undertaken using comparison of the hydrology to analytical solutions and gauged data, which it was found to reproduce with reasonable accuracy.

The impacts of a range of groundwater scenarios on the fluvial and sediment flux discharges from an idealised catchment were tested. Despite the highly simplified nature of the topography and the identical boundary conditions for each simulation, a range of discharge profiles was created. Sediment discharges were found to switch between steady-states under quasi-steady river discharges as the catchments evolved through time. The initial steady-state attained for the majority of scenarios represents no defined river channel. The subsequent move to the next steady-state represents the rapid carving of the main channel. Under certain subsurface conditions (in particular a high specific yield) a nonlinear catchment discharge response is observed despite the uniform forcing factors (precipitation and potential evapotranspiration). Representation of baseflow-return to fluvial flow using uniform baseflow return rates (common in LEMs) is therefore likely to be inaccurate, particularly in catchments with a highly-heterogeneous subsurface. Analysis of the sensitivity scenarios reveals the ability of catchment sediment transport processes to impact surface and subsurface hydrology. Where adequate connectivity exists between surface and subsurface water, the deepening of channels and resultant drop in average river stage reduces surrounding groundwater heads. The sensitivity analysis suggests a high specific yield could potentially return a large volume of water to the surface when the channel is incised. Hydraulic conductivity places a limit on this return by controlling the spatial extent of the impact on groundwater heads; high hydraulic conductivity will create a large area over which groundwater heads are reduced as the river stage drops and low hydraulic conductivity a local reduction.

Analysis of the platform using observational data was limited to the hydrological modules, as sediment flux data was limited at the catchment scale. The calibration technique of matching simulated flow data to gauged data is applicable to any region where continuous records of river flow are present. Further accuracy in the calibration is possible where multiple, distributed, gauging

locations are present across a catchment and with longer flow records that capture a variety of extreme conditions (for example, flooding or drought). For the upper Eden Valley test catchment, calibration was only possible for a single gauging station and although the simulated surface-only flows were well matched to the baseflow separated gauged data, groundwater recession rates were not a good match to the observational data. Obtaining a closer match between observational and simulated groundwater in the upper Eden Valley would be possible through further changes to the distributed hydraulic conductivity and specific yield. However, the calibration process is time consuming and the resources were not available for this study.

5.2. Groundwater and the upper Eden Valley geomorphology

Analysis of the upper Eden Valley sediment flux rates suggests that after two years of simulation there are several differences in regional geomorphology that arise when groundwater is introduced into the system. These can be divided into spatial and temporal differences. Spatial differences in sediment erosion and accretion occur throughout the catchment. When averaged these differences are most apparent at elevations of between 550 and 450 m and can be attributed to increased flow velocities from the addition of baseflow. Temporal differences manifest themselves following large rainfall events. At the event-scale (see Fig. 18), the scenario without groundwater predicts both higher and lower daily sediment discharges in comparison to the groundwater scenario, suggesting that antecedent conditions are highly influential. A time-averaged study may predict similar amounts of erosion, but the inclusion of groundwater is critical for accurate representation of the timing and location of sediment flux events. The averaging effect manifests itself in the similar total catchment sediment flux is observed at the end of the simulation. In general, the groundwater response at the event-scale tends to be more protracted. This is highlighted in Fig. 17, where there are nine extra days in the groundwater simulation where sediment discharge events are at 10 m^3 or below. At the annual scale, the difference in total catchment sediment flux is small, but over decades it could make a significant contribution to the total eroded volume. For studies attempting to recreate the evolution of catchments with high baseflow inputs, the representation of baseflow-return within the fluvial processes that drive sediment discharge rates is important, even if they are represented in an averaged sense. It is also important to note that the predicted increase in extreme rainfall events under future climate scenarios (Bates et al., 2008; Arnell, 2011) should be taken into consideration for studies interested in simulating future landscape morphology.

It is anticipated that application of the CLiDE platform to highly groundwater-dependent alluvial systems with large sediment yields (for example, the Platte River, USA (Knox, 1972); the river Ganges, India (Narayana and Babu, 1983); or the Guadalquivir River, Spain (Lobo et al., 2004)) would show a significant difference in sediment transport with the groundwater module enabled. This would allow an improved assessment of geomorphological evolution over traditional LEM techniques that do not take groundwater into account.

5.3. Caveats and uncertainty

There are assumptions inherent in all environmental modelling systems, as the system being represented needs to be simplified in order to be simulated. Process-based system representation carries fewer assumptions than other techniques, and is central to the modules that make up the CLiDE platform. By sticking to the CA principles and avoiding empirical representation through statistical analysis, the platform is suitable for use in a variety of catchments.

As CA discretises the domain into discrete parts and there is assumed to be no heterogeneity at the sub-cell scale. Any sub-cell scale variation is assumed to be integrated into the cell average value for a particular variable. Time is also divided into sections and therefore sub-time step processes are also assumed to be averaged.

The uncertainty associated with input parameters is often unknown, due to the variety of methods available for producing the parameters and interpolating the data into a fixed grid. As environmental systems are often nonlinear, small changes in the initial conditions may have a large effect on the output of the simulation at advanced time steps. By undertaking a calibration, where model attributes are compared to observed values, these issues will have less of an impact, providing a suitable number of comparisons are made over a significant period of time. For the upper Eden Valley case study, simulated hydrological attributes were calibrated to observed values over a two-year period. There was, however, no attempt made to calibrate the simulated sediment transport as it was assumed that the links between hydrology and sediment transport are adequate, as supported by previous comparison of the sediment transport component to observed data (see Coulthard et al., 2012). If records of sediment transport exist for a catchment the platform may be calibrated to these following the hydrological calibration. To better quantify the impact of the initial parameters on the simulation, an ensemble analysis technique may be employed.

The use of a spin-up period in the initial phase of the modelling process allows the modelled domain to attain a dynamic steady-state. During this period non-forcing hydrological and sediment transport parameters reach a relaxed state, producing quasi-uniform responses to similar meteorological events. The hydrological processes reach this state more rapidly than the sediment transport processes as the early phase represents the building of fluvial systems and the latter phase the distribution of sediment. This allows the spin-up period to compensate for any inaccuracies in the initialisation parameters.

One of the major influences on dynamic morphology that was not captured during this modelling case study is the formation of soil at the bedrock-soil interface. This limits the amount of sediment available for transport within the catchment, and in reality would be controlled by the underlying geology as well as the soil hydrology. As the study covers only two-years of simulation, this process was not deemed important. If a centennial scale study was undertaken this process would need to be captured in the model, or the bedrock layer (non-erodible) would be exposed along the river reach and sediment transport would be constrained by the lateral evolution of the channel only. Currently the only influence that geology exerts on the topography within the model (post initialisation) is through the transport of groundwater and the influence this has on surface hydrology and subsequently sediment transport.

CLiDE is aimed at addressing sub-annual to centennial catchment-scale research. Suitability of the platform as a research tool for millennial scale (or longer) studies is not limited by the numerical representation of the underlying processes, but by available processing power and scalability of the platform under increased parallelisation.

6. Summary and conclusions

A two-dimensional cellular automata platform for exploring the sensitivity of environmental systems over a variety of spatio-temporal scales has been presented to assess the impact of groundwater on regional geomorphological evolution. Physically-based equations were implemented to simulate the flow of surface and subsurface water, which in turn drives sediment transport

between adjacent cells. Surface and subsurface hydrology was coupled through the exchange of recharge to groundwater, and baseflow discharge to rivers. Hydrology and sediment transport, both bedload and suspended, were integrated through river flow velocity and DEM modification. The runtime calculation of several soil hydrological properties makes the resulting platform versatile and easily adaptable for simulating a variety of natural systems under differing forcing scenarios (climatic, geologic or anthropogenic).

Testing of the platform's hydrological components, which have been added to CAESAR-Lisflood to form the CLiDE platform, was underpinned by comparison to analytical solutions, which show the model is stable and convergent. The accuracy of the subsurface hydrological components was found to be good when evaluated against analytical solutions under both transient and steady-state conditions. Testing of the platform in a simple, idealised catchment revealed that the impacts of baseflow-return on catchment sediment discharge manifest themselves in a variety of ways and are therefore difficult to represent in LEMs using uniform rates. The sensitivity analysis also reveals some of the feedbacks that can arise between the hydrological components and catchment morphology, and how these can evolve through a series of transitions between steady-states.

To set some of the model parameters for simulating sediment transport in the upper Eden Valley, the CLiDE platform was calibrated using baseflow separated gauged river data and groundwater level time-series at several locations over a two year period. The parameters derived from calibration appear to be sensible, and it was possible to obtain a good match to the surface river flow data. The matching of the groundwater level time-series was not as good as that achieved in the surface component. However, this was expected as we are representing a complex heterogeneous environmental system using a simplified model.

The input of baseflow into rivers creates a less flashy sediment flux responses to extreme rainfall events. During these events, the transport of sediment is maintained over extended periods, as baseflow keeps river velocities above the minimum sediment transport threshold for longer periods. The groundwater component provides the hydrological system with antecedent conditions, allowing previous events to influence future sediment transport rates. At the event-scale, antecedent rainfall lagged in the system as groundwater can result in a substantial difference in predicted volumes of sediment transport for any particular time. Including a mechanism for capturing the spatial and temporal influence of antecedent rainfall conditions on fluvial flow is therefore essential for shorter-term landscape evolution modelling. Assigning a universal transition point (i.e., defining just how short shorter-term is) where process-based or average baseflow-returns are more appropriate is not possible as it is dependent on the focus of any particular study and the individual catchment characteristics.

Acknowledgements

The authors are grateful to David Macdonald of the British Geological Survey (BGS) for reviewing this paper and returning feedback that led to its improvement. They would also like to acknowledge Dr Jorge Ramirez (currently at Florida Atlantic University) for the preparation of input data, and Henry Holbrook of the BGS for preparation of Fig. 13. This paper is published with the permission of the Executive Director of the British Geological Survey (NERC), and was supported by the Climate and Landscape Change, and the Environmental Modelling research programmes at the BGS.

References

Ahnert, F., 1976. Brief description of a comprehensive three-dimensional process-response model for landform development. Z. Geomorphol. 25, 29–49.
Allen, D.J., Brewerton, L.J., Coleby, L.M., Gibbs, B.R., Lewis, M.A., MacDonald, A.M., Wagstaff, S.J., Williams, A.T., 1997. The physical properties of major aquifers in England and Wales. Br. Geol. Surv. Rep. WD/97/034 (333 pages).
Allen, R., Pereira, L.A., Raes, D., Smith, M., 1998. Crop Evapotranspiration: Guidelines for Computing Crop Water Requirements. FAO, Irrigation and Drainage Paper No. 56. FAO, Rome, Italy.
Arcement, G.J., Schneider, V.R., 1989. Guide for selecting manning's roughness coefficients for natural channels and floodplains. U. S. Geol. Surv. Water-Supply Pap. 2339, 38.
Arnell, N.W., 2011. Uncertainty in the relationship between climate forcing and hydrological response in UK catchments. Hydrol. Earth Syst. Sci. 15, 897–912.
Barkwith, A., Coulthard, T.J., 2014. CLiDE V1.0 User Guide: British Geological Survey Open Report OR/14/011. British Geological Survey, Nottingham, UK, p. 54.
Barry, D.A., Parlange, J.-Y., Li, L., 2000. Approximations for the exponential integral (Theis well function). J. Hydrol. 227, 287–291.
Bates, B.C., Kundzewicz, Z., Wu, S., Palutikof, J., 2008. Climate Change and Water. Technical Paper of the Intergovernmental Panel on Climate Change, Geneva, p. 210.
Bates, P.D., Horritt, M.S., Fewtrell, T.J., 2010. A simple inertial formulation of the shallow water equations for efficient two-dimensional flood inundation modelling. J. Hydrol. 387, 33–45.
Bear, J., 1979. Hydraulics of Groundwater. McGraw-Hill, New York, p. 567.
Bennett, S., Dumble, J.P., Ruxton, C., 2003. The Monitoring of “Poor Aquifers” to Meet the Requirements of the EU Water Framework Directive: Phase 1-review and Scoping Report.
Boorman, D.B., Hollis, J.M., Lilly, A., 1995. Hydrology of Soil Types: a Hydrologically-based Classification of the Soils of the United Kingdom. Report No. 126. Institute of Hydrology, Wallingford, UK.
Butcher, A.S., Lawrence, A.R., Jackson, C., Cunningham, J., Cullis, E., Hasan, K., Ingram, J., 2006. Investigating rising nitrate concentrations in groundwater in the Permo-Triassic sandstone aquifer in the UK. In: Barker, R.D., Tellam, J.H. (Eds.), Fluid Flow and Solute Movement in Sandstones: the Onshore UK Permo-triassic Red Bed Sequence. Geological Society, London, pp. 285–296. Special Publications, 263.
Buttle, J.M., 1994. Isotope hydrograph separations and rapid delivery of pre-event water from drainage basins. Prog. Phys. Geogr. 18 (1), 16–41.
Changnon, S.A., Huff, F.A., Hsu, C.-F., 1988. Relations between precipitation and shallow groundwater in Illinois. J. Clim. 1 (12), 1239–1250.
Chen, S., Doolen, G.D., 1998. Lattice Boltzmann method for fluid flows. Annu. Rev. Fluid Mech. 30 (1), 329–364.
Chopard, B., Masselot, A., 1999. The lattice Boltzmann method: a new approach to computational fluid dynamics and particle transport. Future Gener. Comp. Syst. 16, 249–256.
Coulthard, T.J., 2001. Landscape evolution models: a software review. Hydrol. Process. 15 (1), 165–173.
Coulthard, T.J., Lewin, J., Macklin, M.G., 2005. Modelling differential and complex catchment response to environmental change. Geomorphology 69 (1–4), 224–241.
Coulthard, T.J., Neal, J.C., Bates, P.D., Ramirez, J., de Almeida, G.A.M., Hancock, G.R., 2013. Integrating the LISFLOOD-FP 2D hydrodynamic model with the CAESAR model: implications for modelling landscape evolution. Earth Surf. Process. Land. 38, 1897–1906.
Coulthard, T.J., Ramirez, J., Fowler, H.J., Glenis, V., 2012. Using the UKCP09 probabilistic scenarios to model the amplified impact of climate change on drainage basin sediment yield. Hydrol. Earth Syst. Sci. 16 (11), 4401–4416.
Coulthard, T.J., Van De Wiel, M.J., 2006. A cellular model of river meandering. Earth Surf. Proc. Land. 31, 123–132.
Culling, W.E.H., 1960. Analytical theory of erosion. J. Geol. 68 (3), 336–344.
Daily, P., Ingram, J., Johnson, R., 2006. Groundwater Quality Review: Eden Valley and Carlisle Basin. Environment Agency Report GWQR004 and ESI Report 6438A R1.
Dunne, T., 1988. Hydrology and mechanics of erosion by subsurface flow. In: Back, W., Rosenshein, J.S., Seaber, P.R. (Eds.), Hydrogeology. Geological Society of America, Boulder CO, USA, p. 988.
Eckhardt, K., 2008. A comparison of baseflow indices, which were calculated with seven different baseflow separation methods. J. Hydrol. 352, 168–173.
Einstein, H.A., 1950. The Bed-load Function for Sediment Transportation in Open Channel Flows. Technical Bulletin 1026. USDA, Soil Conservation Science, pp. 1–77.
Fowler, H.J., Tebaldi, C., Blenkinsop, S., 2007. Probabilistic estimates of climate change impacts on flows in the River Eden, Cumbria. In: 10th National Hydrology Symposium: Sustainable Hydrology for the 21st Century. British Hydrological Society, Exeter, UK.
Fox, G.A., Wilson, G.V., Simon, A., Langendoen, E., Akay, O., Fuchs, J.W., 2007. Measuring streambank erosion due to ground water seepage: correlation to bank pore water pressure, precipitation, and stream stage. Earth Surf. Proc. Land. 32 (10), 1558–1573.
Goodrich, D.C., Lane, L.J., Shillito, R.M., Miller, S.N., Syed, K.H., Woolhiser, D.A., 1997. Linearity of basin response as a function of scale in a semi-arid watershed. Water Resour. Res. 33 (12), 2951–2965.
Haan, M.M., Russell, J.R., Powers, W.J., Kovar, J.L., Benning, J.L., 2006. Grazing

management effects on sediment and phosphorus in surface runoff. Rangel. Ecol. Manage. 59, 607–615.
Haitjema, H.M., 1995. Analytic Element Modeling of Groundwater Flow. Academic Press, p. 394.
Hancock, G.R., Coulthard, T.J., Martinez, C., Kalma, J.D., 2011. An evaluation of landscape evolution models to simulate decadal and centennial scale soil erosion in grassland catchments. J. Hydrol. 308, 171–183.
Harr, M.E., 1962. Ground Water and Seepage. McGraw-Hill Book Co., New York.
Hoffmann, T., Thorndycraft, V.R., Brown, A.G., Coulthard, T.J., Damnati, B., Kale, V.S., Middelkoop, H., Notebaert, B., Walling, D., 2010. Human impact on fluvial regimes and sediment flux during the Holocene: review and future research agenda. Glob. Planet. Change 72 (3), 87–98.
Howard, A., McLane, C., 1988. Erosion of cohesionless sediment by groundwater seepage. Water Resour. Res. 24 (10), 1659–1674.
Huang, X., Niemann, J.D., 2006. Modelling the potential impacts of groundwater hydrology on long-term drainage basin evolution. Earth Surf. Proc. Land. 31 (14), 1802–1823.
Keesstra, S.D., Temme, A.J.A.M., Schoorl, J.M., Visser, S.M., 2014. Evaluating the hydrological component of the new catchment-scale sediment delivery model LAPSUS-D. Geomorphology 212, 97–107.
Kelly, P.J., 2012. Subsurface Evolution: Characterizing the Physical and Geochemical Changes in Weathered Bedrock of Lower Gordon Gulch, Boulder Creek Critical Zone Observatory. Master's thesis. University of Colorado.
Kinnell, P.I.A., 2010. Event soil loss, runoff and the Universal soil loss equation family of models: a review. J. Hydrol. 385 (1–4), 384–397.
Kirchner, J.W., Feng, X., Neal, C., 2000. Fractal stream chemistry and its implications for contaminant transport in catchments. Nature 403 (6769), 524–527.
Knox, J., 1972. Valley alleviation in southwestern Wisconsin. Ann. Assoc. Am. Geogr. 62 (3), 401–410.
Laity, J.E., Malin, M.C., 1985. Sapping processes and the development of theater-headed valley networks on the Colorado Plateau. Geol. Soc. Am. Bull. 96, 203–217.
Lange, J., Greenbaum, N., Husary, S., Ghanem, M., Leibundgut, C., Schick, A.P., 2003. Runoff generation from successive simulated rainfalls on a rocky, semi-arid, Mediterranean hillslope. Hydrol. Process 17, 279–296.
Lobo, F.J., Sanchez, R., Gonzalez, R., Dias, J.M.A., Hernandez-Molina, F.J., Fernandez-Salas, L.M., Diaz del Rio, V., Mendes, I., 2004. Contrasting styles of the Holocene highstand sedimentation and sediment dispersal systems in the northern shelf of the Gulf of Cadiz. Cont. Shelf Res. 24, 461–482.
Malby, A.R., Whyatt, J.D., Timmis, R.J., Orr, H.G., 2007. Long-term variations in orographic rainfall: analysis and implications for upland catchments. Hydrolog. Sci. J. 52 (2), 276–291.
Margolus, N., Toffoli, T., Vichniac, G., 1986. Cellular-automata supercomputers for fluid dynamics modeling. Phys. Rev. Lett. 15 (16), 1694–1696.
Mayes, W.M., Walsh, C.L., Bathurst, J.C., Kilsby, C.G., Quinn, P.F., Wilkinson, M.E., Daugherty, A.J., O'Connell, P.E., 2006. Monitoring a flood event in a densely instrumented catchment, the upper Eden, Cumbria, UK. Water Environ. 20 (4), 217–226.
Merritt, W.S., Letcher, R.A., Kakeman, A.J., 2003. A review of erosion and sediment transport models. Environ. Modell. Softw. 18, 761–799.
Metha, A., Barker, G.C., 1994. The dynamics of sand. Rep. Prog. Phys. 57 (4), 385–416.
Murray, A.B., Paola, C., 2003. Modelling the effect of vegetation on channel pattern in bedload rivers. Earth Surf. Proc. Land. 28, 131–143.
Narayana, D.V.V., Babu, R., 1983. Estimation of soil erosion in India. J. Irrig. Drain. Eng. 109 (4), 419–434.
Neal, J., Schumann, G., Fewtrell, T., Budimir, M., Bates, P., Mason, D., 2011. Evaluating a new Lisflood-FP formulation with data from the summer 2007 floods in Tewkesbury, UK. J. Flood Risk Man. 4, 88–95.
Pazzaglia, F.J., 2003. Landscape evolution models. Dev. Quatern. Sci. 1, 247–273.
Payn, R.A., Gooseff, M.N., McGlynn, B.L., Bencala, K.E., Wondzell, S.M., 2012. Exploring changes in the spatial distribution of stream baseflow generation during a seasonal recession. Water Resour. Res. 48, W04519.
Ravazzani, G., Rametta, D., Mancini, M., 2011. Macroscopic cellular automata for groundwater modelling: a first approach. Environ. Modell. Softw. 26 (5), 634–643.
Roache, P.J., 1976. Computational Fluid Dynamics. Hermosa, Albuquerque, NM. Rev. 1976.
Rothman, D.H., 1988. Cellular-automaton fluids: a model for flow in porous media. Geophys. 53 (4), 509–518.
Rushton, K.R., 2003. Groundwater Hydrology: Conceptual and Computational Models. John Wiley and Sons Ltd, West Sussex, England.
Sklash, M.G., Favolden, F.N., 1979. The role of groundwater in storm runoff. J. Hydrol. 45, 45–65.
Somers, J.A., 1993. Direct simulation of fluid flow with cellular automata and the lattice-Boltzmann equation. Appl. Sci. Res. 51 (1–2), 127–133.
Toffoli, T., 1984. Cellular automata as an alternative to (rather than an approximation of) differential equations in modeling physics. Phys. Nonlinear Phenom. 10 (1–2), 117–127.
Tooth, S., Jansen, J.D., Nanson, G., Coulthard, T.J., Pietsch, T., 2008. Riparian vegetation and the late Holocene development of an anabranching river: Magela Creek, northern Australia. GSA Bull. 120 (7–8), 1021–1035.
Tucker, G.E., Hancock, G.R., 2010. Modelling landscape evolution. Earth Surf. Proc. Land. 35 (1), 28–50.
Van De Wiel, M.J., Coulthard, T.J., Macklin, M.G., Lewin, J., 2007. Embedding reach-scale fluvial dynamics within the CAESAR cellular automaton landscape evolution model. Geomorphology 90, 283–301.
Van De Wiel, M.J., Coulthard, T.J., Macklin, M.G., Lewin, J., 2011. Modelling the response of river systems to environmental change: progress, problems and prospects for palaeo-environmental reconstructions. Earth Sci. Rev. 104 (1–3), 167–185.
von Neumann, J., 1951. The general and logical theory of automata. Cereb. Mech. Behav. 1–41.
von Neumann, J., 1966. Theory of Self-reproducing Automata. University of Illinois Press, Urbana, IL.
Wang, J.F., Anderson, M.P., 1982. Introduction to Groundwater Modelling. Freeman, San Francisco, CA, USA.
Wilcock, P., Crowe, J., 2003. Surface-based transport modelling for mixed-size sediment. J. Hydraul. Eng. 129 (2), 120–128.